

Civil Engineering Journal

(E-ISSN: 2476-3055; ISSN: 2676-6957)

Vol. 11, No. 09, September, 2025



Pre- and Post-Cracking Resistance of Steel Fiber Reinforced Concrete Flexural Members with GFRP Bars

Shatha D. Mohammed ^{1*}, Rafaa M. Abbas ¹, Hamza M. Salman ¹, Nazar K. Oukaili ¹, Abbas A. Allawi ¹

¹ Department of Civil Engineering, University of Baghdad, Baghdad 17001, Iraq.

Received 26 April 2025; Revised 17 July 2025; Accepted 11 August 2025; Published 01 September 2025

Abstract

This research investigates the pre- and post-cracking resistance of steel fiber-reinforced concrete specimens with Glass Fiber Reinforced Polymer (GFRP) bars subjected to flexural loading. The purpose is to modify the ductility and cracking resistance of GFRP-reinforced beams, which are prone to early cracking and excessive deflections instigated by the low modulus of elasticity of GFRP. Six self-compacting concrete specimens (1500×240×200 mm), incorporating steel fibers of two lengths (25 mm and 40 mm) with varying distribution depths, were tested to assess their structural performance. The results indicate significant enhancements in cracking resistance, stiffness, energy absorption, ductility, and flexural strength. Tested beams reinforced with 40 mm-long steel fibers exhibited a 23.9%-24.2% development in the ultimate moment capacity associated with the steel-reinforced specimens, whereas those with 25 mm fibers showed smaller increases (2.7%-3.1%). The cracking resistance improved by up to 33.3% in beams with 40 mm-long fibers and by 16.67%-20% in those with 25 mm-long fibers, associated with a non-fibrous GFRP specimen. Additionally, the inclusion of 40 mm hooked-end steel fibers significantly enhanced ultimate deflection, with peak deflections increasing by 30.2%-44.8% compared to steel-reinforced beams. Fibrous GFRP-reinforced beams exhibited up to 154% higher energy absorption under ultimate load than a non-fibrous GFRP beam. All fibrous GFRP-reinforced beams achieved deformationbased ductility indices between 4.2 and 6.9, exceeding the minimum threshold of 4 for adequate deformability. These findings confirm that incorporating 40 mm steel fibers significantly improves the structural behavior of GFRP-reinforced concrete specimens, offering valuable insights for optimizing their design.

Keywords: GFRP Bars; Steel Fibers; Self-Compacting Concrete; Cracking Resistance; Energy Absorption; Ductility Index.

1. Introduction

Ordinary steel bars are utilized to reinforce conventional concrete flexural specimens since it had high tensile strength and notable ductility. Steel reinforcement's poor resistance to corrosion is its primary flaw. Because of the concrete's alkalinity, the steel is initially shielded from corrosion, which typically leads to a durable functional construction. On the other hand, concrete constructions exposed to harsh environments, such as chlorides, temperature, and moisture, have reduced alkalinity, which accelerates the corrosion of reinforcing bars. Concrete eventually deteriorates and loses its serviceability due to steel bar corrosion [1]. Fiber-reinforced polymers (FRP) are an effective alternative for reinforcing bars in concrete constructions. Since FRP bars are noncorrosive and have greater tensile strength in comparison to steel bars, they are more advantageous when utilized as reinforcement in structural concrete members [2-4].

^{*} Corresponding author: shatha.dh@coeng.uobaghdad.edu.iq





© 2025 by the authors. Licensee C.E.J, Tehran, Iran. This article is an open access article distributed under the terms and conditions of the Creative Commons Attribution (CC-BY) license (http://creativecommons.org/licenses/by/4.0/).

Glass fiber-reinforced polymer (GFRP) bars were considered a favorable candidate in concrete construction reinforcement since they addressed corrosion-related difficulties [5]. Among the other advantageous qualities that contributed to GFRP bars' expanding application were their nonmagnetic qualities, low weight, and high tensile strength [6-8]. Furthermore, GFRP reinforcement offers significant advantages in constructions that require reinforcement with non-metallic characteristics, such as those enclosing medical apparatus or those that need a member's strength-to-weight ratio to be high [9].

As a consequence of several in-depth studies, design standards and norms for reinforced concrete buildings using FRP bars have been issued. Among these are the ACI 440.1R-15 [10] and CSA-S806-12 [11]. The ACI code-440.11-22 [12] is a recent code that specifies particular requirements for GFRP bars. Many researchers investigated the structural performance of GFRP-reinforced concrete flexural members. According to the research findings of Alsayed et al. [13], the GFRP-reinforced beams had a linear behavior until failure caused by concrete crushing and a failure technique that complied with a design criterion regulating flexural failure. Tavares et al. [14] demonstrated that the comparatively low rupture strain and elasticity modulus of the GFRP bars were two essential parameters that affected the flexure capability of the GFRP-reinforced concrete beam. In addition, mild steel bars exhibited a clear yield plateau before failure, but GFRP bars displayed a linear response until failure with no warning signs.

The structural performance of simply-supported concrete members reinforced with various fiber-reinforced polymer bars was studied by many researchers [15–20]. The outcomes show that the beams reinforced with GFRP bars appeared to crack earlier than the beams reinforced with steel bars. Additionally, related to steel reinforced beams, those reinforced with GFRP bars encountered a more significant deflection under the same applied service load [19, 20]. Test results of reinforced concrete beams with steel and GFRP bars simultaneously were presented by Saraswathy & Dhanalakshmi [21] and Moawad & Fawzi [22]. The findings indicated that increasing the reinforcing ratio of GFRP bars resulted in fewer but wider cracks. The GFRP bars had an impact on the beams' stiffness, and beams with smaller GFRP reinforcement ratios displayed significant deformations. The structural behavior of a one-way concrete slab reinforced with steel and GFRP bars under fire exposure was studied by Mohammed & Shatha [23, 24]. By evaluating a fire-exposed model reinforced by GFRP bars of different concrete covers, the ideal concrete cover was found. Furthermore, the experimental findings demonstrated how the failure mechanism is affected by the GFRP replacement ratio.

Increases in the main GFRP reinforcement ratio in concrete beams have been found to improve the member's overall stiffness by reducing mid-span deflection, improving load-carrying capacity, and narrowing crack widths. Since GFRP rebars do not yield, shear failure, which can be a brittle failure mode, can occur in GFRP-reinforced concrete beams [25]. For GFRP-RC beams, the recommended failure mechanism is hence concrete crushing. In other words, ACI 440.1R-15 [10] states that FRP-reinforced concrete beams should be over-reinforced such that their failure is due to concrete crushing rather than rebar rupture. According to Swamy & Al-Noori [26], the existence of steel fibers allows for the use of high-strength steel with a yield strength of 700 MPa while controlling crack width and deflection within allowable bounds. Along with having a high modulus of elasticity and tensile strength, steel fibers' favourable geometrical characteristics and availability also significantly reduce concrete cracking problems and improve crack resistance [27–29].

Concrete features, hence, have a noteworthy influence on the system's ductility. The use of various discrete fibers can mitigate the detrimental impact of the GFRP bars' inherent brittleness on serviceability. Incorporating short steel fibers (SF) into the concrete mix might be a more effective, practical, and simple solution to the ductility issue. Concrete's mechanical properties, toughness, and ductility have all been improved by researchers adding fibers to the concrete, particularly to make it tougher and to recover the concrete characteristics of brittleness and cracking [9].

The fiber's bridging inhibits the propensity for crack width and length to continue growing by reducing stress concentration in the cracking area [30]. Because of the crack-bridging effect, adding discrete fibers to concrete has been reported to be useful in enhancing its different properties [31–35]. According to the researchers' findings, SF is highly effective at resisting deformation that occurs through all stages of loading, preventing cracks from widening and spreading, joining cracks to strengthen the cracked tension zone, improving inelastic distortions, increasing the ductility at failure, and enhancing the beams' shear capacity and its ultimate flexural strength [9].

Even though it is now evident that adding SF may significantly enhance the concrete section's engineering capabilities, steel's propensity to rust in specific situations is the main reason for searching for a replacement reinforcing material. Therefore, the primary benefit of utilizing FRP bars rather than steel may be ignored by incorporating SF into the concrete mixture [9]. According to earlier research, SF corrosion will only occur on the concrete's surface skin when the concrete is well-compacted and has a compressive strength greater than 21 MPa at 28 days of age. It appears that corrosion does not spread over two to three millimeters away from the surface once the surface fibers have corroded [36]. Meanwhile, there isn't a continuous channel of conductivity between different concrete regions for developed or stray currents from an electromotive potential since the fibers are short, discrete, and seldom touch one another. Thus, the ductility issue concerning the use of FRP bars as reinforcement for concrete construction may be determined in a diversified and more useful way by using SF in FRP beams [9].

In recent decades, FRC, or fiber-reinforced concrete, has provided superior immovability against high-strain loading associated with ordinary concrete and also a better dominance over plastic shrinkage and cracking propagation. Adding fibers to concrete has been demonstrated in several studies to considerably modify its properties. Therefore, for ordinary and lightweight concrete members, the presence of fibers enhanced their ductility, toughness, flexural and torsional strength, compressive and tensile strength, and energy absorption capacity [37–39].

The impact of steel fiber volume and geometrical characteristics on the ability of reinforced high-strength concrete (HSC) beams without transverse reinforcement to withstand shear was studied by Yoo et al. [40]. By adding steel fibers and increasing their volume percentage up to 1.0%, the authors reported that the shear strength of HSC beams without transverse reinforcement rose dramatically, leading to a shear strength that was around 1.7 times greater. In relation to the increase in shear strength, a greater fiber aspect ratio improved the deformability of HSC beams without transverse reinforcement and their resistance to shear failure.

The post-cracking performance of GFRP-RC beams under flexure and shear was inspected through the use of discrete fibers. Both flexure and shear performance have been found to be enhanced by the inclusion of fibers, whether synthetic or steel [41]. The ductility and post-cracking stiffness of steel fibers are often more than those of macrosynthetic fibers [41, 42]. High and ultra-high-performance fiber-reinforced concrete beams reinforced with fiber-reinforced polymer (FRP) and steel bars have been studied for their flexural behavior. It was found that post-cracking stiffness, first cracking load, and load capacity were among the improved flexural performances due to the increased FRP reinforcement ratio [43–48]. The flexural behavior of lightweight fiber-reinforced ultra-high performance concrete (LUHPC) beams reinforced with GFRP and high-strength steel bars was investigated by Li et al. [49]. Investigating the effects of various reinforcement materials (steel bars and GFRP) and reinforcement ratios (0.59%, 1.27%, and 1.94%) on the flexural performance of LUHPC beams under static load was the primary aim of the investigation. Results revealed that the current specifications ACI 440.1R-15 [10] and CSA S806-12 [11], accurately foretell the cracking load (moment) and deflections associated with the service load for the GFRP-reinforced LUHPC beams. Still, they dramatically underrate the flexural strength and associated deflections. As the reinforcement ratio increased, predictions began to become less conservative.

Numerous investigations on the flexure or shear response of GFRP RC beams with various combinations, such as hybrid reinforcements [50, 51], the inclusion of discrete fibers [9, 52], or both [53], are clearly visible in the literature. Studies upon the flexure or shear performance of GFRP RC beams containing discrete steel fibers are, nonetheless, quite limited. There aren't many studies that explore how fiber insertion affects the response of GFRP-reinforced concrete (RC) beams. Consequently, the goal of this work is to investigate the influence of steel fiber length and the depth of the layer at which the fibers are dispersed on the performance of concrete beams. The methodology employed in this study consisted of an experimental program involving the testing and statistical analysis of six RC beams, both fiber-reinforced and non-fiber-reinforced. The primary objective was to investigate the influence of several parameters, including the type of reinforcement (steel or GFRP), the presence of steel fibers (fiber-reinforced versus non-fiber-reinforced), steel fiber length (25 mm and 40 mm), and the depth of the fiber-reinforced layers.

GFRP-reinforced concrete flexural members may experience significant cracking widths and deflections due to the bars' mechanical characteristics. As a result, in the design process of GFRP reinforced concrete members, the serviceability limit conditions are often the governing factor. By incorporating steel fibers into the concrete mix, this study seeks to modify the serviceability and strength capacity of GFRP-reinforced concrete beams. The current study aims to estimate how the cracking, deformability, and strength of steel fiber-reinforced concrete specimens with GFRP bars are affected by the characteristics of steel fiber (such as length) and the depth of the layer at which the fibers are dispersed in relation to the entire cross-sectional depth of the specimen.

2. Experimental Work Details

Six scaled-down beam samples were fabricated and tested to explore the flexural performance of fiber-reinforced concrete beams with GFRP bars. Two reference beams without fibers were cast; one was reinforced with steel bars, and the other with GFRP bars. Short and long steel fibers (SF) were positioned in the lower third part of the cross-sectional depth of two of the beam samples, whereas fibers were positioned across the whole depth of the beam in the other two. In terms of cracking, stiffness, toughness, energy absorption capacity, and flexural strength, the improved structural performance that was achieved by the addition of steel fiber was demonstrated here.

2.1. Concrete Constitutive Materials

Figure 1 shows the flowchart of the research methodology through which the objectives of this study were achieved. Self-compacting concrete (SCC) with a target cylinder compressive strength of 55 MPa was used to fabricate all of the test specimens. The tested specimens were manufactured using ordinary Portland cement (OPC) type (I) that complies with the ASTM C150 [54] limitations. Table 1 shows the chemical characteristics of cement,

whereas Table 2 shows its physical properties. In accordance with ASTM C33/C33M-16 requirements, crushed aggregate with a nominal particle size of 12.5 to 4.75 mm was utilized as the coarse aggregate [55]. Table 3 and Figure 2 display the coarse aggregate's physical, chemical, and sieve analysis data. Natural fine aggregate was used; it was compatible with the ASTM C33/C33M [55] requirements. Sieve analysis, physical, and chemical properties are shown in Table 3 and Figure 2. Silica fume, which complies with ASTM C 1240-20 [56] requirements, was used as an additive. At seven days, the silica fume's accelerated pozzolanic strength activity index was 118%. Water-reducing admixture type F, which conforms to ASTM C494/C494M-19 [57], was added to the concrete mix to produce self-consolidating concrete (SCC).

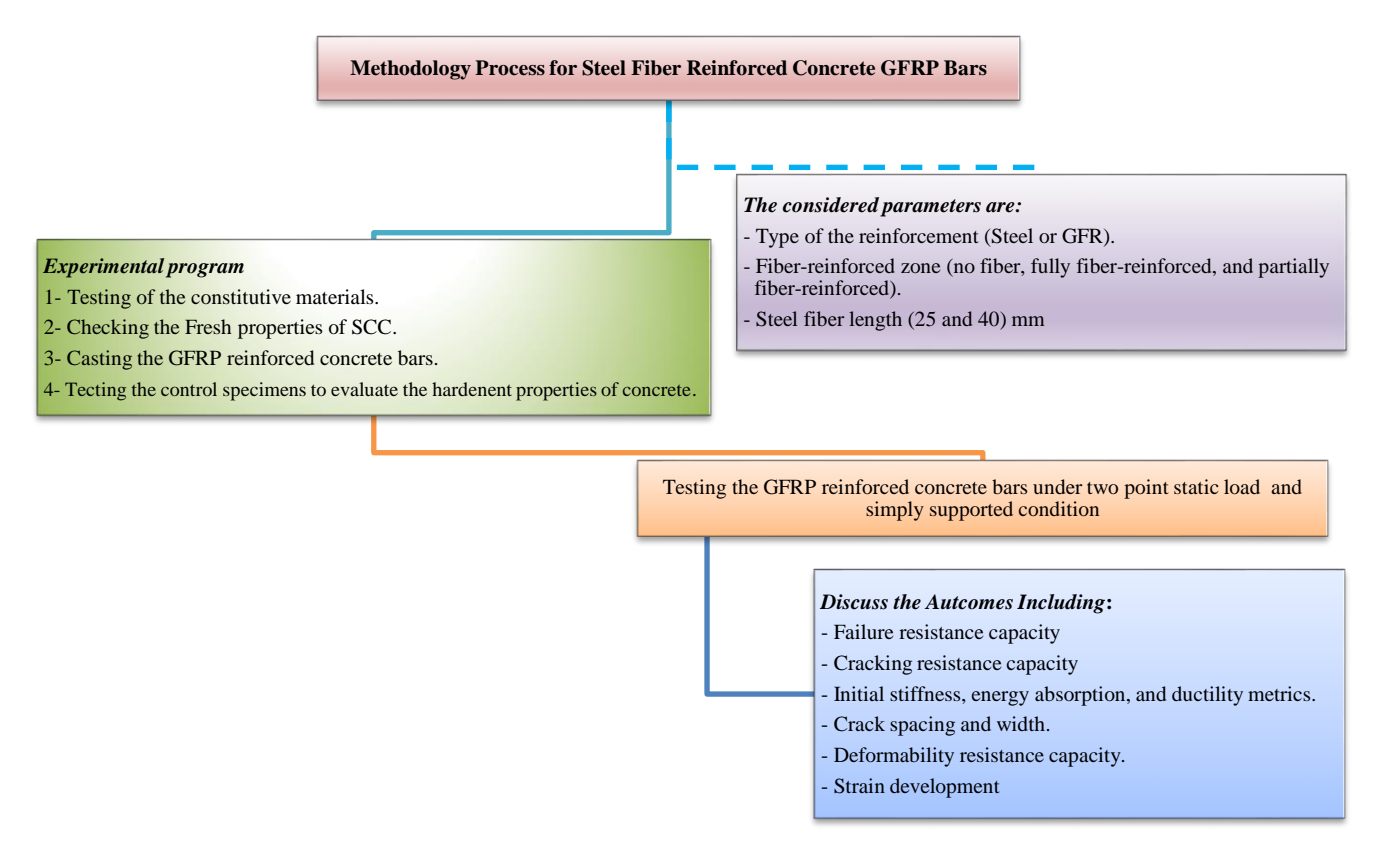


Figure 1. Flowchart for the research methodology

Table 1. Ordinary Portland cement (OPC) chemical composition

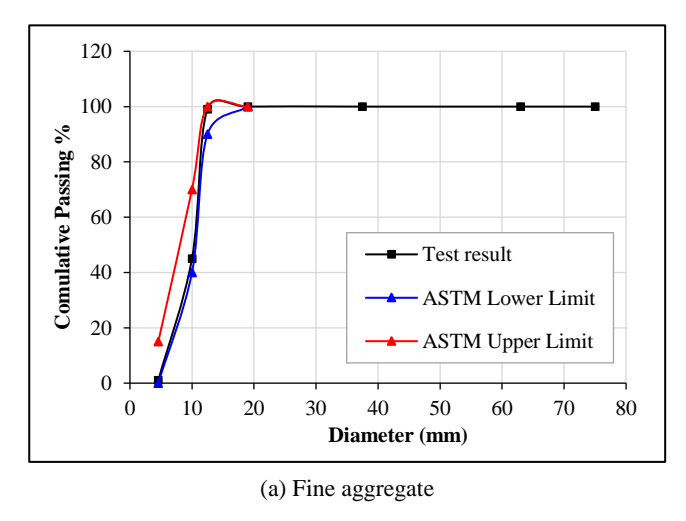
Chemical Composition	Results	Limits of ASTM C150
Lime (CaO)	69.50	
Silica (SiO ₂	23.50	
Alumina (Al ₂ O ₃)	4.82	
Iron Oxide (Fe ₂ O ₃)	2.61	
Magnesia (MgO)	2.83	≤ 6.0 %
Sulfate (SO ₃)	2.05	\leq 3.5 if $C_3A \geq 8\%$
Insoluble residue (I.R)	0.88	≤ 1.5 %
Loss on Ignition (L.O.I)	2.10	≤ 3.5 %
Main Compou	nd of OPC	
Tri Calcium Silicate (C ₃ S)	62.30	
Di Calcium Silicate (C ₂ S)	20.07	
Tri Calcium Aluminate (C ₃ A)	8.36	
Tera Calcium Aluminate Ferrite (C ₄ AF)	7.93	

Table 2. Ordinary Portland cement (OPC) physical properties

Physical Property	Result	Limits of ASTM C150		
Specific surface area m²/kg (Blain method)	330	≥ 260		
Initial setting time (minutes)	120	≥ 45 minutes		
Final setting time (hour: minute)	4:38	≤ 375 minutes		
Compressiv	e Strength			
at 7 days, (MPa)	18.50	≥ 12		
at 3 days, (MPa)	30.60	≥ 19		

Table 3. Aggregate characteristics

	Coarse aggregat	e	Fine aggre	gate	
Sieve size (mm)	Passing (%)	Limits of ASTMC33	Sieve size (mm)	Passing (%)	Limits of ASTM C33
75.0	100	Not limited	9.5	100	100
63.0	100	Not limited	4.75	96	95 –100
37.5	100	Not limited	2.36	80	80 - 100
19.0	100	100	1.18	60	50 - 85
12.5	12.5 99 90-100		0.6	35	25 - 60
10.0	45	40-70	0.3	13	5 - 30
4.57	1	0-15	0.15	4	0 - 10
			0.075	1	0-3
Property	Test Result		Property	Test Result	
Specific gravity	2.58		Specific gravity	2.66	
Absorption	0.75%		Absorption	0.69%	
Sulfate content (SO ₃)	content (SO ₃) 0.065%		Sulfate content (SO ₃)	0.41%	
Dry-rodded density	$1610~kg/m^3$		Dry rodded density	1625 kg/m^3	
			Fine particles passing through the sieve 75 μm	2.78%	



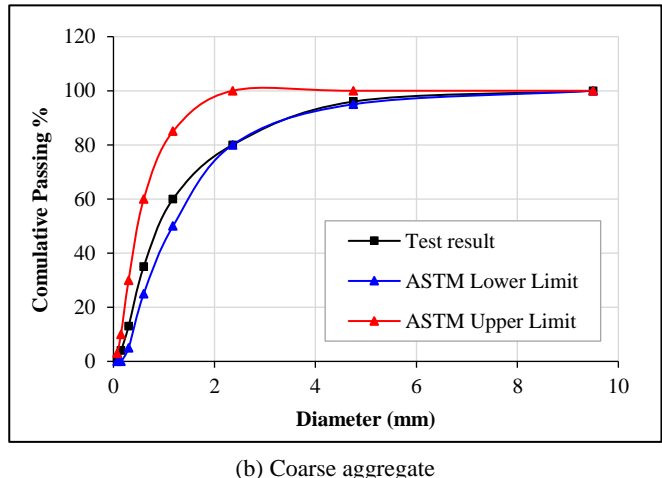


Figure 2. Granulation curves for the used aggregate

2.2. Reinforcement (Steel Bars, GFRP Bars, and Steel Fibers)

The reference beam was reinforced with longitudinal mild steel bars of two different diameters, namely 10 mm and 12 mm. As indicated in Table 4, it was found that the steel bars' properties are compliant with ASTM A615M [58]. In five tested beams, GFRP bar with a diameter of 10 mm was used as the main longitudinal flexural reinforcement. In all tested beams, two-legged stirrups prepared using 10 mm diameter steel bars were used as transverse reinforcement. Finally, to produce steel-fiber reinforced self-compacting concrete, two types of hooked-end steel fibers with circular cross-sectional configuration were utilized, as seen in Figure 3. The steel fibers' length (L) and diameter (D) were measured with an accuracy of 0.01 mm using an inner diameter micrometer. The (L/D) ratio yields the aspect ratio ($\tilde{\chi}$). Table 4 lists all of the mechanical and physical characteristics of the steel bars, GFRP bars, and steel fibers (SF) under consideration.

Table 4. Reinforcement details

No.	Element	Length (mm)	Diameter (mm)	Sectional area (mm²)	Yield Strength (MPa)	Ultimate Strength (MPa)	Elongation (%)	Modulus of Elasticity (MPa)	Density (kg/m³)	Aspect ratio
1	Steel-bars	-	10.0	76.06	433.0	615.0	12.0	200000	7860	-
2	Steel-bars	-	12.0	112.92	443.5	624.7	14.0	200000	7860	-
3	GFRP-bars	-	10.0	78.7	1205	-	2.45	48280	2804	-
4	Steel-fibers	40	0.55	-	1300	-	-	200000	7800	73
5	Steel-fibers	25	0.30	-	2400	-	-	200000	7800	83





(a) 4 cm-length

(b) 2.5 cm-length

Figure 3. Hooked-end steel fibers that implemented in the SCC of the tested beams

2.3. Mix Design and Fresh Self-Compacting Concrete Properties

The adopted self-compacting mixture of concrete constituent materials and their proportions are displayed in Table 5. The fresh characteristics of the SCC mix were evaluated by five tests as disclosed in Table 6. Segregation Index (SI) percentage, L-box (H2/H1), V-funnel, T500 mm, and slump flow results were all within the limits of EFNARC 2005 [59].

Table 5. Mix proportions of self-compacting concrete (SCC)

Cement (kg/m³)	(kg/m^3) (kg/m^3)		Water (kg/m³)	Silica fume (kg/m³)	Water reducing admixture (kg/m³)
576	760	900	162	24	8.4

Table 6. Fresh characteristics of self-compacting concrete (SCC)

Mix	Test outcomes and limits of specifications									
- IVIIA	Slump flow (mm)	T _{500 mm} (sec)	V- funnel (sec)	L-box (H2/H1)	Segregation index (SI) (%)					
SCC	740	2.9	9.5	0.91	14.7					
(EFNARC 2005) Limits	SF1 (550 - 650) SF2 (660 - 750) SF3 (760 - 850)	VS1≤2 VS2>2	VF1 ≤ 8 VF2 (9 - 25)	≥ 0.8	$SR1 \le 20$ $SR2 \le 15$					

2.4. Characteristics of Tested Specimens

All of the tested specimens had the same geometrical arrangement, dimensions, and concrete cylinder compressive strength. While the compressive strength was 56 MPa, the dimensions of the tested specimens were 1500x240x200 mm for length, depth, and width, respectively. Two reinforcing configurations were accounted for the reinforcement details of the tested specimens. Steel bars were used to reinforce the beam in the first configuration, with $2\phi12$ mm and $1\phi10$ mm of steel bars used at the bottom of the tension zone of the section and $2\phi10$ mm at the top of the compression zone. The second arrangement displays specimens with GFRP reinforcement, whose structural design complies with ACI code 440.11-22 requirements [12]. GFRP was used in a $2\phi10$ mm as top and bottom reinforcement arrangement. The two configurations that were chosen provided almost the same moment capability for the tested beams.

For concrete beams that are reinforced with steel or GFRP bars, the shear reinforcement used was the same of $\phi 10$ mm @ 90 mm, which satisfied the flexure failure mode condition rather than the shear failure mode condition.

The hardened properties of the SCC are displayed in Table 7, while Figure 4 shows the dimensions and details of the tested specimens. As seen in Figure 5, steel fiber (SF) also had an impact on specimen categorization; three scenarios were chosen based on the fiber-reinforced zone (no fiber, fully fiber-reinforced, and partially fiber-reinforced), see Table 8. Additionally, two hooked steel fiber lengths (25 and 40 mm) were taken into consideration in order to explore how the fiber length affected the tested specimens' structural behavior. All of the investigated specimens with SF had a fiber

volume fraction of 1.25 percent (i.e., 98 kg per cubic meter of concrete). The selection was informed by prior literature and confirmed through trial mixes designed to evaluate both the fresh and hardened properties of the concrete. Given that self-compacted concrete was used, the high workability and flowability facilitated uniform dispersion of steel fibers, effectively preventing issues such as segregation or clumping.

Table 7. Mechanical properties of self-compacting concrete (SCC)

Concrete	Steel fiber	Steel fiber volume	Comp	ressive strength	Splitting	g tensile strength	Modulus of elasticity		
type	length (mm)	length (mm) fraction (%)		$ \frac{f'_c}{(\text{MPa})} \qquad \Delta = \frac{f'_c - f'_{c,ref}}{f'_{c,ref}} \ (\%) $		$\Delta = \frac{f_t - f_{t,ref}}{f_{t,ref}} \ (\%)$	E _c (MPa)	$\Delta = \frac{E_c - E_{c,ref}}{E_{c,ref}} (\%)$	
Without SF	-	-	56.0 -		4.0	-	31500	-	
With SF	40	1.25	68.5 22		6.8	70	37500	19	
With SF	25	1.25	64.0	14	5.2	30	34620	10	

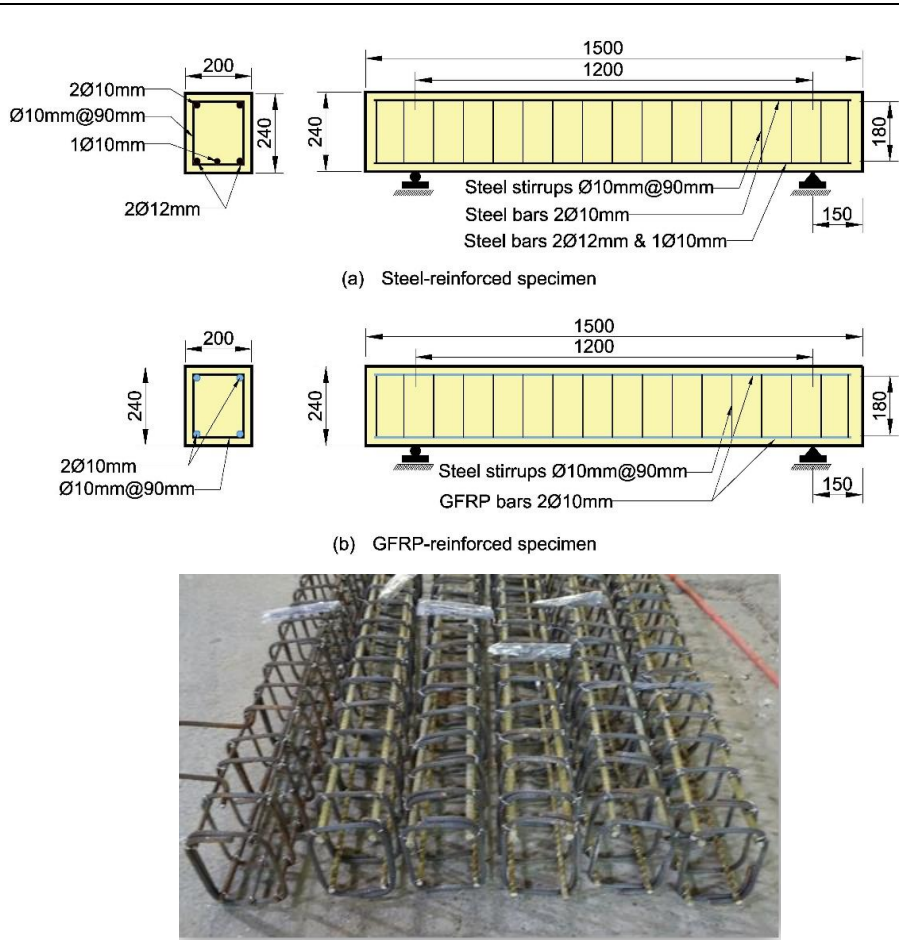


Figure 4. Reinforcement details of tested beams (all dimensions are in mm)

(c) Overall view of reinforcement cages

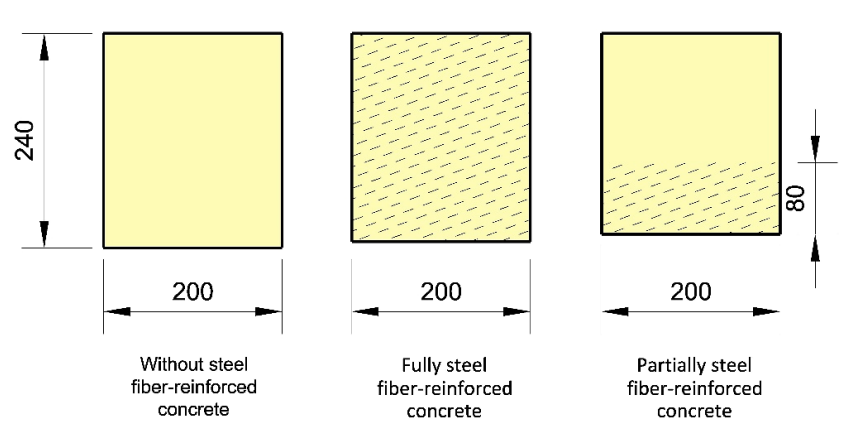


Figure 5. Steel fibers distribution categories (all dimensions are in mm)

Across full depth

Across full depth

One-third of the depth

One-third of the depth

Specimen

designation

SNF **GNF**

GF4H

GF2.5H

GF4H/3

GF2.5H/3

GFRP

GFRP

GFRP

GFRP

Type of flexural reinforcement	Type of shear reinforcement	Steel fiber length (mm)	Steel fiber-reinforced concrete layer
Steel	Steel	-	-
GFRP	Steel	-	-

40

25

40

25

Table 8. Characteristics of tested beams

Steel

Steel

Steel

Steel

According to ASTM C39/C39M [60], ASTM C496/C496M [61], and ASTM C469/C469M [62], the average compressive strengths, tensile splitting strength, and modulus of elasticity of the plain self-compacting concrete and steel fiber-reinforced self-compacting concrete were measured using three cylindrical specimens measuring 150 mm × 300 mm for each variable. The compressive strength, tensile splitting strength, and elasticity modulus of the plain SCC increased from their lowest values of 56 MPa, 4 MPa, and 31500 MPa, respectively, with the addition of steel fibers. This is due to the fact that the steel fibers create interfacial linkages that stop cracks from widening and propagating. With SF of 40 mm-long, steel fiber-reinforced concrete showed the highest values of 68.5 MPa, 6.8 MPa, and 37500 MPa, respectively. It is worth mentioning that the composite concrete cylinders with SF of 40 mm and 25 mm long, respectively, achieved increases in compressive strength, splitting strength, and modulus of elasticity of 22%, 70%, and 19%, and 14%, 30%, and 10%, respectively, in comparison to the concrete mix without steel fibers.

2.5. Experimental Test Process

Initially, the specimen surfaces were prepared by painting them white. A 30 \times 30 mm mesh was then created in order to obtain a precise crack observation. As seen in Figure 6, electrical strain gauges were also mounted on the concrete surface throughout the depth of the tested component at the chosen midspan section as part of the specimen preparation process. The specimen was then placed within the testing rig in an arrangement that achieved a simply supported scheme by utilizing hemispherical rigid supports (a hinge and a roller), with a spacing of 1200 mm between these supports. A pure bending span of 300 mm and two shear spans of 450 mm each were created by distributing the generated load equally between two sections using a steel I-section spreader to transmit the applied static load in two concentrated load systems. A 1500-kN hydraulic jack and a 2000-kN load cell, respectively, generated and monitored the applied static load.

The applied load, vertical deflection, initial crack width, crack pattern and propagation, and strain in steel bars, GFRP bars, and concrete were among the several characteristics that were included in the test measures that were taken into consideration. To quantify the vertical deflection at the specimen midspan section, a linear variable differential transducer (LVDT) with a 7.5 cm stroke was employed. Additionally, a computerized system was used to automatically record the test results. A 5.0 kN incremental load step was monotonically applied until the failure, at which point the development of the cracks was accurately monitored and recorded. The details of the electrical strain gauges that were used are shown in Figure 6, and the test setup and the instruments and devices that were utilized are shown in Figure 7.

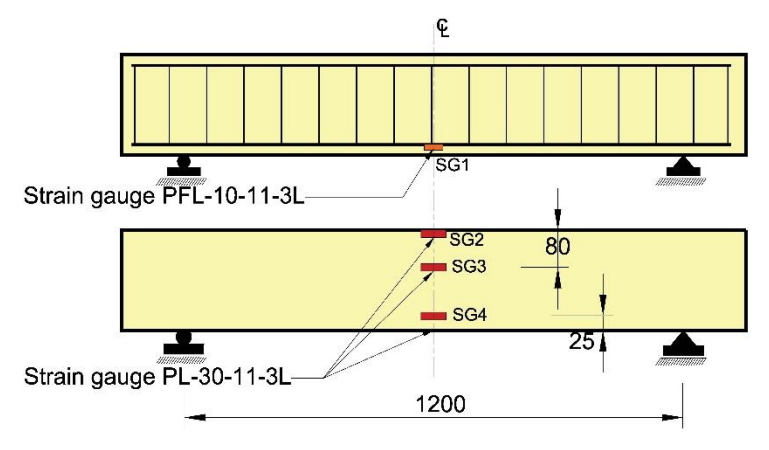


Figure 6. Adopted locations of the strain gauges (all dimensions are in mm)

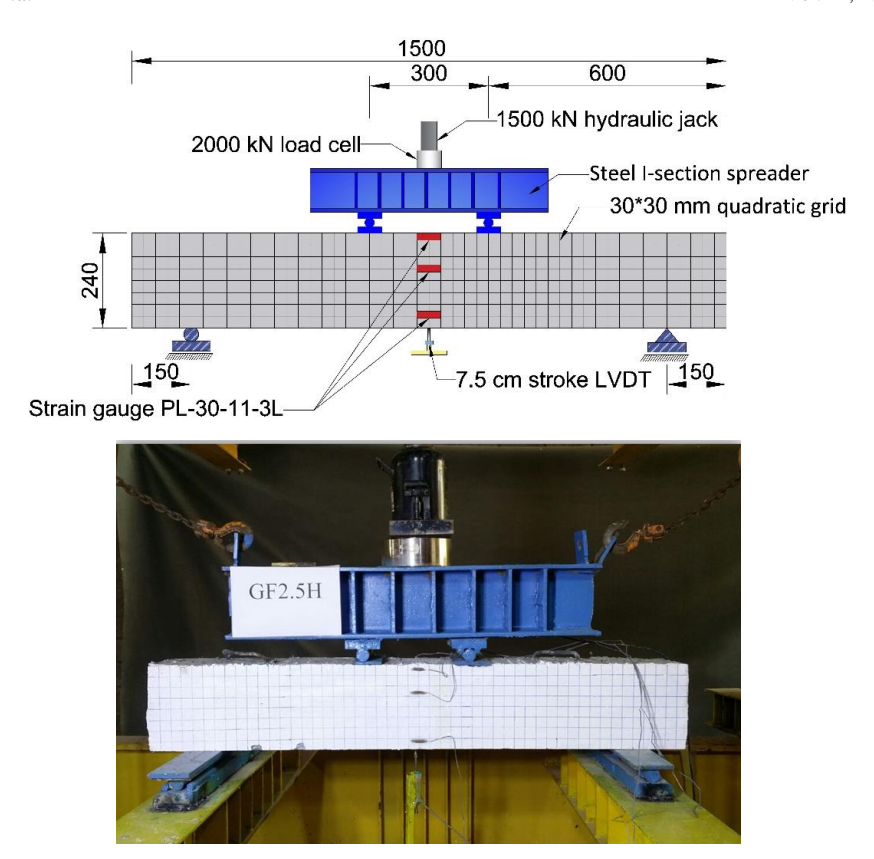


Figure 7. Experimental test layout and instrumentations (all dimensions are in mm)

3. Results and Discussion

The main goals of the experimental program were to find out how using GFRP main bars compared to traditional steel main bars influenced the performance of reinforced concrete beams under monotonic static load, how adding steel fiber (SF) of two different lengths—25 and 40 mm—to the concrete mix impacted the results, and how the depth of the steel fiber reinforced concrete layer affected the outcomes that were obtained. In order to accomplish an effective investigation into the effect of the factors indicated, a number of structural aspects were taken into consideration. The moment and deflection that occurred at the onset of the cracking process, at the ultimate service load, and at the ultimate load, in addition to the stiffness, absorbed energy, and ductility, were among the structural characteristics that were taken into consideration. The investigation was extended to identify the relationships between moment-deflection, moment-crack width, and moment-strain distribution.

3.1. Failure Resistance Capacity

Table 9 lists the ultimate loads, which are the highest loads determined for each beam by the load cell employed with the data gathering system. For the steel-reinforced beam SNF with self-compacting concrete that had no steel fibers in its mix, the beam's ultimate moment was 36.68 kN.m. It should be mentioned that the two longitudinal reinforcement configurations in beams SNF and GNF were chosen to attain almost comparable moment capabilities during the design phase of the experimental work.

 $\frac{P_{cr}-P_{cr,ref}}{P_{cr,ref}}$ (%) $\frac{P_{u}-P_{u,ref}}{P_{u,ref}}$ (%) M_{cr} Beam P_u (kN) $P_{cr,ref}$ ID (kN.m) (kN.m) (1)* (2)* (4)* (1)*(2)* (3)*(3)*(4)*SNF 9.00 163.0 Ref. 36.68 **GNF** 30 6.75 -25.0 Ref. 164.2 36.95 0.7 Ref. GF4H 202.5 40 9.00 0.00 33.33 11.11 2.56 45.56 24.2 23.33 20.54 0.30 GF2.5H 8.10 -10.00 20.00 Ref. 2.86 168.0 37.80 3.1 2.31 Ref. 0.36 36 GF4H/3 39 8.78 -2.5030.00 11.43 Ref. 201.9 45.43 23.9 22.96 20.61 Ref. GF2.5H/3 167.4 35 7.88 -12.5016.67 Ref. 37.67 1.95 Ref.

Table 9. Load and moment outcomes at cracking and failure stages

Note: (1) Comparisons with SNF to discover the impact of using GFRP bars or the GFRP bars with SF; (2) Comparisons with GNF to explore the impact of the implementation of SF; (3) Comparisons between GF4H and GF2.5H, also between GF4H/3 and GF2.5H/3 to explore the impact of the length of SF; (4) Comparisons between GF4H and GF4H/3, also between GF2.5H and GF2.5H/3 to discover the impact of the depth of the layer at which the fibers are dispersed in relation to the entire cross-sectional depth of the beam.

Consequently, specimen GNF's ultimate moment was just 0.7% higher than the steel-reinforced beam SNF's, which confirmed the intended target. Although many researchers stated that there was no discernible improvement in ultimate strength at a greater volume fraction of 1.0% due to the negative impacts of steel fiber addition, namely increase in inhomogeneous fiber distribution and air content [40, 63], the results of this study presented an alternative scenario. The ultimate moments of specimens GF4H and GF4H/3 were, respectively, 24.2% and 23.9% larger than those of the steel-reinforced specimen SNF. However, specimens GF2.5H and GH2.5H/3 showed an insignificant effect of the steel fibers, with ultimate moments that were 3.1% and 2.7% greater than SNF, respectively. This finding demonstrates the significance of selecting the appropriate SF length.

In comparison to specimen GNF, the ultimate moment of specimens GF4H, GF4H/3, GF2.5H, and GF2.5H/3 was greater for 23.33%, 22.96%, 2.31%, and 1.95%, respectively. This increase may be explained by the steel fibers' ability to inhibit the formation and spread of cracks, which impacts the tensile and compressive strengths of the concrete matrix and significantly reduces the phenomenon of concrete crushing, particularly in specimens with steel fibers that are 40 mm long. As an alternative to 40 mm-long steel fibers, the use of short 25 mm-long hooked-end steel fibers in self-compacting concrete was inadequate to tangibly enhance the moment capacity of the GFRP-reinforced concrete beams. For this conclusion to be supported, further experimental data from various tested beams with different cross-sectional configurations, spans, concrete compressive strengths, steel fibers of other shapes and volume fractions, longitudinal reinforcement ratios, and depths of the layer where the steel fibers are distributed are required.

The fiber length has a major impact on the ultimate moment enhancement. Compared to shorter steel fibers, longer steel fibers permit a larger flexural crack opening prior to failure. In comparison to specimens GF2.5H and GF2.5H/3, the ultimate moments of specimens GF4H and GF4H/3 were 20.54% and 20.61% higher, respectively. Furthermore, the improvement in the ultimate moment is less noticeable when the depth of the layer where the steel fibers are spread is greater than one-third of the total cross-sectional depth of the beam. The ultimate moments of specimens GF4H and GF2.5H were only slightly higher than those of GF4H/3 and GF2.5H/3, by 0.30% and 0.36%, respectively.

3.2. Cracking Resistance Capacity

In general, the dimensions of the cross section and the concrete's strength determine the cracking moment. Thus, based on the testing results, adding steel fibers can increase the cracking moment. The outcomes of the experiments generally indicated that the mechanical properties of the materials utilized, such as the kind of concrete mix across the section and the type of the longitudinal main reinforcing bars determine the onset and later the progress of any beam cracks. The entire cracking propagation process of the tested beams may be roughly summed up in the following: (a) The beam is in the elastic region prior to cracking initiation, showing an approximate linear relationship between the deformability and the load imposed. When beams reinforced with steel (SNF), GFRP bars (GNF), or GFRP bars with steel fiber-reinforced concrete layers attain the cracking strain under load, the weakest spot—the bottom of the pure bending span or its surrounding area—showed the development of at least one randomly positioned vertical crack. (b) In the beam's pure bending span, the number of cracks expanded to certain amount with increasing load before stabilizing, while the spacing between cracks remained comparatively constant. (c) After the pure bending span's cracking number reached a certain limit, the cracks expanded vertically and their depth stabilized at a particular load level. (d) As loading increased, the flexural primary cracks formed and propagated toward the cross-section's compression zone, which ultimately led to the failure of the tested beams by either crushing the concrete in the compression zone (as is the case with all GFRP-reinforced beams) or yielding the steel bars in the tension zone (as is the case with SNF).

Due to the varied bonding behavior, lower modulus of elasticity, anisotropy, and reduced stiffness of the GFRP bars, the cracking moment in specimen GNF was 25% lower than that of the steel-reinforced beam SNF, as shown in Table 9 [64, 65]. In specimens GF4H and GF4H/3, the cracking moment was equivalent to and 2.5% lower than that of the steel-reinforced specimen SNF, respectively. Specimens GF2.5H and GH2.5H/3, on the other hand, had cracking moments that were 10% and 12.5% lower than SNF, respectively.

The presence of steel fibers of 40 mm long and 73 aspect ratio, with a volume fraction of 1.25%, notably enhanced the cracking moment of the GFRP-reinforced concrete beams, with the advantages becoming more gradual with steel fibers of 25 mm long and 83 aspect ratio with the same volume fraction. The cracking moment of specimens GF4H, GF4H/3, GF2.5H, and GF2.5H/3 was higher for 33.33%, 30%, 20%, and 16.67%, respectively, than the cracking moment of specimen GNF. This may be explained by the fact that the steel fibers' bonding and mechanical interlocking effectively increased the concrete matrix's tensile and compressive strengths, which in turn significantly increased the cracking moment.

Meanwhile, the improvement of the cracking moment is only marginally affected by the fiber length. The cracking moments of specimens GF4H and GF4H/3 were 11.11% and 11.43% higher, respectively, than those of specimens GF2.5H and GF2.5H/3. It is pertinent to note that when the depth of the layer where the steel fibers are distributed exceeds one-third of the beam's entire cross-sectional depth, the improvement in cracking moment becomes less pronounced. The specimens GF4H and GF2.5H improved their cracking moments by 2.56% and 2.86%, respectively, in comparison to GF4H/3 and GF2.5H/3.

3.3. Crack Pattern and Failure Modes

The failure modes and the progress of cracking of all the tested specimens are depicted in Figure 8. Three categories can be used to categorize the failure modes seen in the tested beams of the present study.

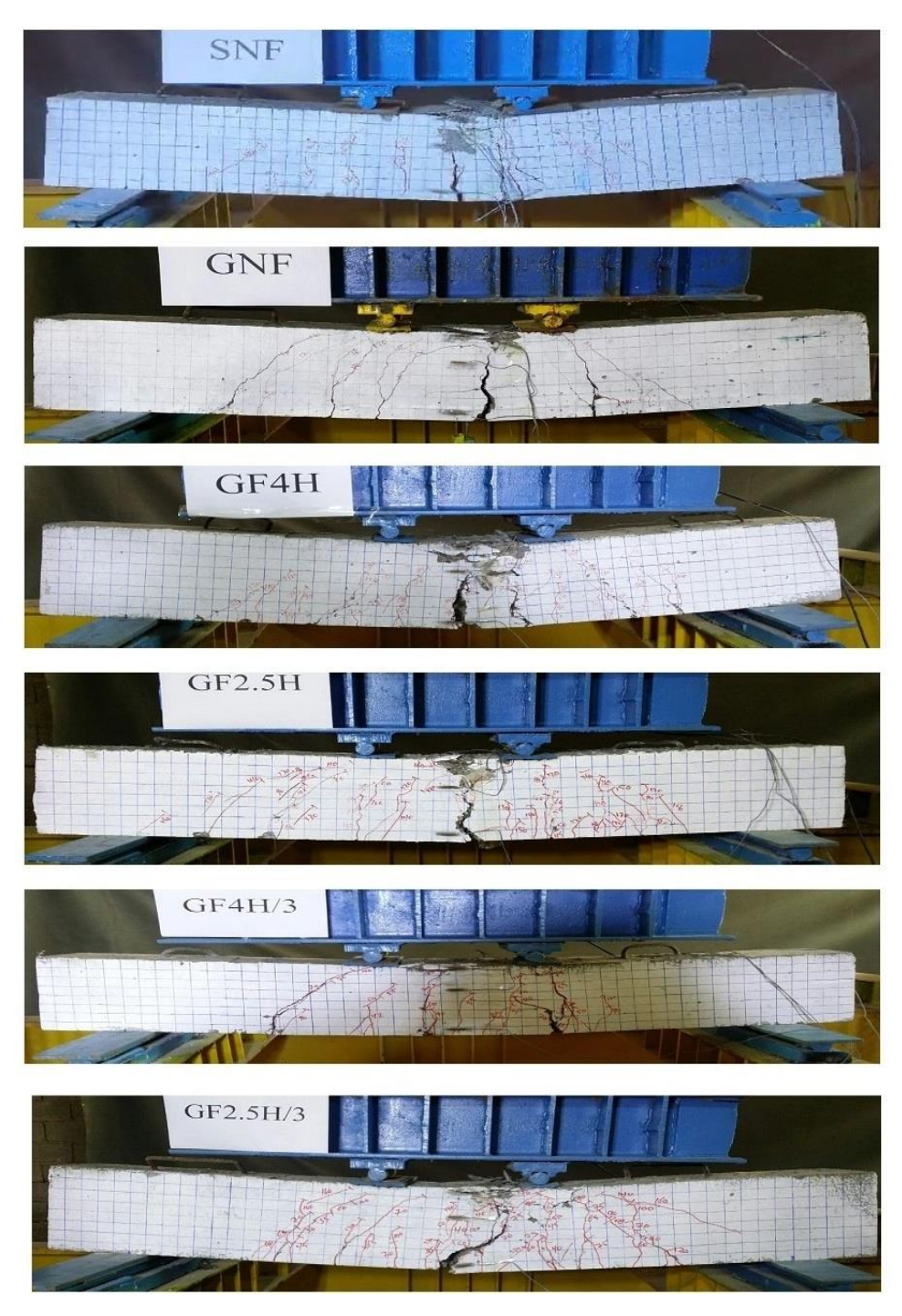


Figure 8. Failure mode and crack pattern for tested specimens

The first was ductile flexural failure, sometimes known as tension failure, which was noted in specimen SNF where the concrete in the compression zone was crushed once the longitudinal tension steel bars yielded, starting the failure process. This failure was accompanied by two significant flexure cracks.

The second, which was seen in beam GNF, was flexural failure accompanied by two significant shear cracks. Both SNF and GNF experienced flexural failure that was coupled with crushing of the concrete at the farthest, from the neutral axis, fibers in the compression zone.

The third, which was flexural failure combined with local top crushing of concrete, was exhibited in beams GF4H, GF2.5H, GF4H/3, and GF2.5H/3.

The pure bending span of each of the six tested beams was where the first cracks developed, and the stresses were subsequently concentrated in a single major flexure crack. Worthy to note that after the concrete in the compression zone began to crackle, cracks were no longer illustrated or documented for the authors' safety during testing. To guarantee the safety of the testing procedure, terminate applying the load once the whole concrete in the compression zone has been completely damaged.

The first loading phase caused many vertical cracks to occur inside the pure bending span of the SNF beam, which lacks the support of steel fibers. In GNF beam flexural cracks first appeared and spread throughout it. When the applied load progressed to 75% of the peak load, a new flexure cracking began to form and eventually transformed into a shear crack, and the shear spans of the GNF specimen developed long diagonal cracks that expanded toward the locations of the applied loads at higher load levels. Consequently, the main flexure crack rapidly propagated, and concrete crushing occurred.

The distribution of cracks in GF4H, GF2.5H, GF4H/3, and GF2.5H/3 beams was comparable. Nevertheless, because of the steel fibers' ability for deformation, these beams, which had GFRP bars as their primary reinforcement, showed signs of ductile fracture following peak loading. In the GF4H and GF2.5H beams, four to six major cracks progressively developed in the pure bending span after the moment that the concrete cracked. No new cracks developed in the pure bending span, and one of these cracks expanded vertically to three-fifths and three-fourths, respectively, of the beam height when the load reached about 70% Pu. The expanded crack's width then rapidly increased and oblique cracks developed in the shear spans. Consequently, the concrete reached the ultimate compressive strain and was crushed when horizontal cracks developed in the compression zone as the peak load approached.

Five to six flexure cracks gradually appeared in the pure bending span of the GF4H/3 and GF2.5H/3 beams as soon as the concrete cracked. When the load reached almost 70% Pu, one of such cracks propagated vertically to seven-eighths and three-fourths of the beam height, respectively. Then, inclined cracks formed in the shear spans as the width of the widened crack quickly expanded. As the peak load approached, horizontal cracks appeared in the compression zone, causing the concrete to attain the ultimate compressive strain and collapse. Compared to beam GNF, it's important to remember that the addition of discrete steel fibers to the tested beams GF4H, GF4H/3, GF2.5H, and GF2.5H/3 enhanced the crack distribution's intensity and homogeneity, see Figures 8 and 9, as well as the specimens' susceptibility to react to the applied load. This improved the level of the local damage that developed in the midspan compression zone and allowed the specimen to sustain higher applied loads, especially for specimens with SF that was 40 mm-long.

This is due to the fact that the randomly distributed steel fibers in concrete could effectively change the direction of stress transmission, enabling the test specimens to swiftly move from localized stress to overall stress quickly, enhancing the phenomenon of the stress concentration, preventing the development of macroscopic cracks, and inhibiting the propagation of unstable cracks [66]. As a result, the tested beams were able to keep functioning with a considerable number of cracks under the imposed loads. In addition to the longitudinal GFRP rebars, which primarily resisted the tensile force at the flexural crack surfaces, the steel fibers also resisted the flexural cracks, which are typically vertical with respect to the tensile force direction. The discontinuous steel fibers also assisted in resisting a higher tensile force in conjunction with the GFRP rebars.

In steel fiber-reinforced concrete (SFRC) beams, steel fibers are regarded as a crucial reinforcements for restraining inclined shear cracks [40]. As per the present test results, the bridging ability of the steel fibers seems more clearly a determining factor in the shear resistance of GFRP-reinforced concrete beams. Accordingly, the mechanical properties of hardened concrete were improved by the steel fibers, particularly the compressive strength, which increases the concrete's permissible shear strength, and the tensile strength, which controls the crack formation. As a result, even though inclined shear cracks developed in GF4H, GF2.5H, GF4H/3, and GF2.5H/3, the greater crack-resisting potential of the hooked-end steel fibers prevented them from widening.

3.4. Crack Spacing and Width

A map illustrating the position and direction of the cracks on the front side of the experimental beam was generated after it had first developed; this can be seen in Figure 9. Also, the load values that matched to the cracking extension phase were recorded. The cracking distribution map clearly exhibited that the beams with hooked-end steel fibers had a greater cracking density than the other two beams without steel fibers.

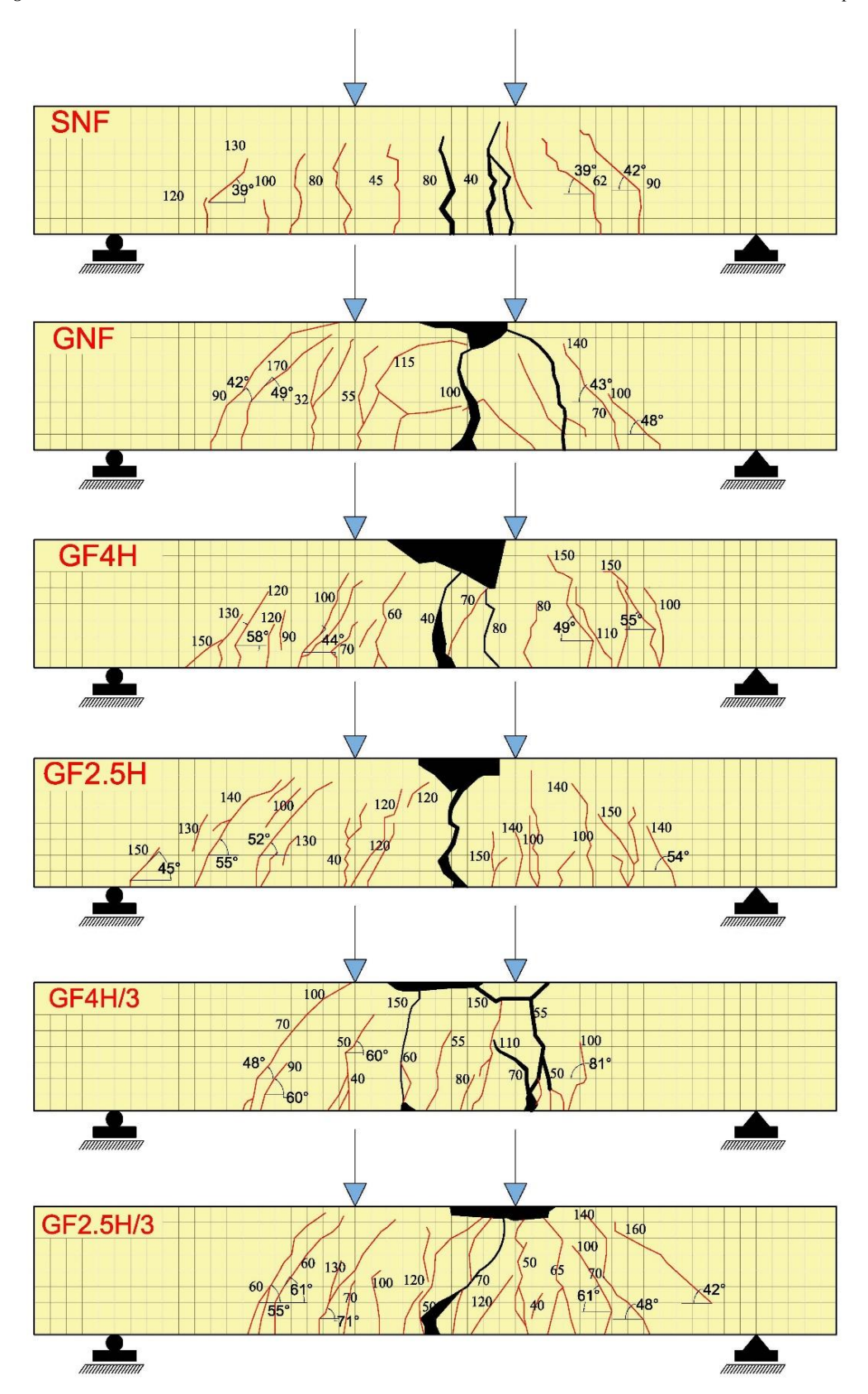


Figure 9. Crack distribution and angles of inclination for tested specimens

In addition to having a significant impact on the stress distribution, the number of cracks at the failure stage is a crucial indicator of the failure mode, ductility, and warning signals of sudden failure.

All tested beams' crack behavior is displayed in Figure 10 and Table 10, along with the correlations between the bending moment and the maximum crack width, average spacing between cracks, and the number of generated cracks. It should be mentioned that for the tested beams, the width of the cracks addressed in this work was at the extreme tensile concrete fiber level.

15

10

5

0

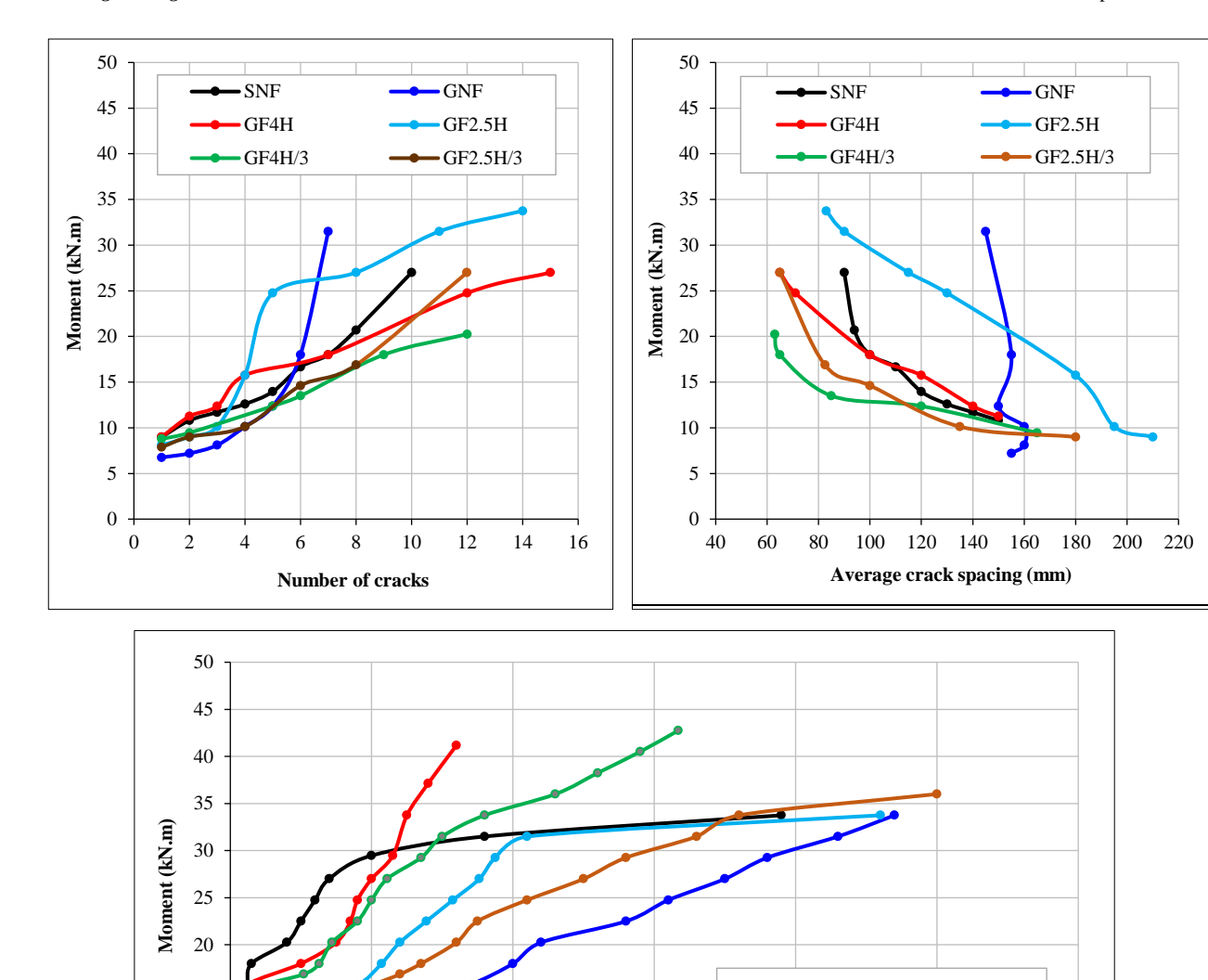


Figure 10. Cracking process of tested specimens

3 Maximum crack width (mm)

2

-SNF

GF4H

GF4H/3

-GNF

-GF2.5H

GF2.5H/3

Table 10. Steel fiber effect on the number of developed cracks

Beam	Total number	Change	Change relative to	No. of flexural	Range of distance		vice stage • 0.65 <i>M</i> _u	Ultin	mate stage
ID	of cracks	relative to SNF (%)	GNF (%)	cracks	cracks (mm)	M (kN.m)	Crack width (mm)	<i>M_u</i> (kN.m)	Crack width (mm)
SNF	10		+42.9	5	90-100	23.6	0.55	36.68	6
GNF	7	-30.0		4	150-160	23.9	3.00	36.95	9
GF4H	15	+50.0	+114.3	8	30-90	29.5	1.15	45.56	17
GF2.5H	14	+40.0	+100.0	8	30-60	24.8	1.50	37.80	10
GF4H/3	12	+20.0	+71.4	7	30-60	29.3	1.35	45.43	14
GF2.5H/3	12	+20.0	+71.4	7	30-60	23.9	2.10	37.67	11

According to the results, GFRP bars decreased the number of cracks created at the failure stage by 30% when steel reinforcement was substituted. In comparison to the SNF beam, the GNF beam had a larger crack width and average crack spacing, fewer cracks, and faster crack formation. This is mostly due to the GFRP bars' weak bonding, low elasticity modulus, and increased slip.

Additionally, the test findings in Table 10 demonstrated that the addition of steel fibers significantly increased the crack number values created in comparison to the GNF specimen. When steel fiber was added, the resulting cracking process behaved better. For a given moment, the maximum crack width and the average crack spacing values of beams GF4H, GF2.5H, GF4H/3, and GF2.5H/3 were reduced as steel fibers were utilized in contrast to non-fiber reinforced concrete beam GNF. This fact is explained by the bridging effect that steel fibers generated, which increased the flexural stiffness of the tested beams and further restrained the crack development.

In comparison to the GFRP-reinforced concrete specimen (GNF), Table 10 demonstrates how the length of the hooked-end steel fibers and the depth of the steel fiber-reinforced concrete layer affect the number of cracks, average crack spacing, and maximum crack width at the ultimate loading stage.

Evidently, the number of cracks that were formed and the distance between them were not considerably impacted by the steel fiber's length. The number of cracks produced at ultimate load in specimens GF4H and GF2.5H was higher for 114.3 and 100 percent, respectively, than in specimens GNF; however, it was only higher for 71.4% in specimens GF4H/3 and GF2.5H/3. The crack spacing in the GNF specimen ranged from 150 to 160 mm. In contrast, GF4H had crack spacing ranging from 30 to 90 mm, whereas GF2.5H, GF4H/3, and GF2.5H/3 had crack spacing ranging from 30 to 60 mm.

A more noticeable impact on the tested beams' cracking process was observed with the depth of the steel fiber-reinforced concrete layer. Instead of only using the bottom third of the whole depth, it was more efficient to extend the steel fiber-reinforced concrete layer throughout the whole depth. Comparing the GF4H and GF2.5H specimens to the SNF specimen, the total number of cracks at failure was 50% and 40% more, respectively, whilst the GF4H/3 and GF2.5H/3 specimens had 20% more cracks. These findings showed that the steel fibers had a positive impact on the flexural behavior of the GFRP-reinforced beam.

It should be noted that, due to aesthetic and durability considerations, large beam crack widths are not permitted in the service condition. For steel-RC or FRP-RC structures, the maximum crack width of the tension face was specified in ACI 318-19 [67] as 0.41 mm and CSA S806:12 (R2021) [11] and CAN/CSA-S6:19 [68] as 0.5 mm, respectively. In reinforced concrete (RC) structures, the American code ACI 318-19 [67] specifies that the permissible crack width is between 0.1 and 0.41 mm, depending on the exploitation environment and the exposure criteria. In the meanwhile, FRP-RC beams may have a maximum crack width of 0.5 mm in accordance with Canadian standards CSA S806:12 (R2021) [11] and CAN/CSA-S6:19 [68], with an associated ultimate service load value that should not be less than 30% of the ultimate applied load (P_u).

It is important to note that no single value for the ultimate service load in reinforced concrete (RC) and FRP-RC beams is explicitly provided by ACI 318-19, CSA S806:12 (R2021), or CAN/CSA-S6:19. Instead, they provide recommendations for aspects of serviceability such as load combinations, crack width control, and deflections in order to design for both strength and serviceability. Usually, 30-60% of the ultimate load capacity (Pu) represents the service load in practical design. The ultimate service load, which is around $65\% \sim 67\%$ of the ultimate load capacity (P_u), has been recognized by several studies [49].

The experimental outcomes explored that at a service moment of 20.25, 10.58, 17.33, 13.73, 16.65, and 12.60 kN.m, respectively, specimens SNF, GNF, GF4H, GF2.5H, GF4H/3, and GF2.5H/3 achieved a crack width of 0.41 mm. Accordingly, these loads represented 55.2%, 28.6%, 38%, 36.3%, 36.7%, and 33.5% Mu, see Table 11. These findings show that the majority of specimens are below the maximum service load allowed by ACI 318-19 [67], suggesting possible concerns with its serviceability.

Beam -	Maximum crack 0.41 mn		Maximum crac 0.50 m			tion relative to	Moment varia GNF	tion relative to
Designation	Corresponding service moment M_{ser} (kN.m)	$\frac{M_{ser}}{M_u}$ (%)	Corresponding service moment M_{ser} kN.m)	$\frac{M_{ser}}{M_u}$ (%)	@ Max. crack width of 0.41 mm	@ Max. crack width of 0.50 mm	@ Max. crack width of 0.41 mm	@ Max. crack width of 0.50 mm
SNF	20.25	55.2	22.50	61.3				
GNF	10.58	28.6	11.25	30.5	-47.8	-50		
GF4H	17.33	38.0	18.00	39.5	-14.4	-20	+63.8	+60.0
GF2.5H	13.73	36.3	14.18	37.5	-32.2	-37	+29.8	+26.0
GF4H/3	16.65	36.7	16.88	37.1	-17.8	-25	+57.4	+50.0
GF2.5H/3	12.60	33.5	13.50	35.8	-37.8 -40		+19.1	+20.0

Table 11. Service load corresponding to maximum permissible crack width

Upon reaching a crack width of 0.5 mm, the SNF, GNF, GF4H, GF2.5H, GF4H/3, and GF2.5H/3 beams were subjected to moments of 22.5, 11.25, 18, 14.18, 16.88, and 13.5 kN.m, respectively. As a result, all evaluated beams' cracking widths in the service condition could meet their respective limitations. These loads accounted for 61.3%, 30.5%, 39.5%, 37.5%, 37.1%, and 35.8% P_u , see Table 11. These results confirm that all specimens meet the 30% M_u criterion of the CSA S806:12 (R2021) [11] and CAN/CSA-S6:19 [68].

However, the significant variation in service load percentages among specimens suggests that material properties and reinforcement type influence crack development and corresponding service loads. Practically speaking, the results highlight how crucial it is to ensure that service load levels match the crack width restrictions set by the relevant codes. The Canadian standards give a greater allowable limit for FRP-RC beams, recognizing the changes in material behavior, whereas ACI 318-19 imposes stricter crack width restriction for RC beams. The experimental findings demonstrate that in order to preserve structural integrity and durability under various environmental circumstances, beams must be designed to balance service load capacity with crack width constraints.

In conclusion, for RC and FRP-RC structures to be serviceable and durable, adherence to crack width limitations is crucial. The experimental results show that additional improvements in reinforcement design may be required to guarantee compliance with serviceability standards under varied load situations, even though they typically do not coincide with the requirements of the ACI 318-19 code.

Figure 8 illustrates the relationship between the crack width and the applied moment for different comparison conditions. In general, the crack width increased approximately at a constant rate as the applied moment increased for all the tested beams, but this rate increased rapidly near the failure stage.

The maximum crack width behavior during the post-cracking stage is impacted by the addition of hooked-end steel fiber, as Figure 8 illustrates. It is evident that the moment-maximum crack width curves for beams with 25 mm- or 40 mm-long steel fibers start to deviate from those of beams SNF and GNF after the first cracking moment was applied. So that they were limited by the GNF beam's lower curve and the SNF beam's upper curve. The presence of the steel fiber-reinforced concrete layer in the bottom third of the depth of the beam section caused the moment-maximum crack width curves to diverge to the side of the GNF curve. Meanwhile, the deviation of the curve was to the side of the SNF curve when the steel fiber-reinforced concrete layer covered the entire depth of the beam's cross-section. Also, the moment-maximum crack width curves of beams with 40 mm-long steel fibers were obviously closer to the SNF curve, regardless of how deep the steel fiber-reinforced concrete layer was. In contrast, the curves for beams with steel fibers that were 25 mm-long were nearer the GNF curve. As the bridging impact was greater than that of the short fibers, this illustrates how effectively extending the fiber length to a certain practical value may reduce the crack width. Furthermore, at the same loading level, specimens GF2.5H and GF2.5H/3 encountered wider cracks than all other specimens, with the exception of beam GNF.

Additionally, it was found that the crack widths of the specimens GF4H and GF4H/3 were less than those of the specimens GF2.5H and GF2.5H/3, respectively, when the applied moment exceeded 15 kN.m. This was because the 25 mm-long steel fibers gradually pulled out or ruptured at a rate higher than that of the 40 mm-long steel fibers, causing the cracks to widen. Longer steel fiber, as in specimens GF4H and GF4H/3, produced nearly identical load-crack width curves from the moment the crack first appeared until the loading at which the crack extension exceeded one-third of the depth of the beam section, as shown in Figure 8. Also, it is evident that the maximum crack width for a given steel fiber length decreases with increasing steel fiber distribution depth. This phenomenon is explained by the steel fiber's bridge effect, which restricts the crack's growth following beam cracking.

3.5. Deformability Resistance Capacity

Figure 11 displays the moment-deflection diagrams for all the tested beams. At the ultimate moment, it is evident that the steel-reinforced concrete beam (SNF) exhibited ductile behavior, but the GFRP-reinforced concrete beam (GNF) experienced brittle behavior. While the SNF beam has three distinctive points—compression concrete crushing, tension steel bar yielding, and tension concrete cracking; the GNF beam's moment—deflection curve exhibits bilinear character.

In the initial stage of loading the concrete matrix mostly sustains tensile stress prior to concrete cracks. So, all beams with the two longitudinal reinforcement types (steel and GFRP), as well as those with and without steel fibers, have comparable bending stiffness characteristics, and the mid-span deflection develops linearly with increasing moment. It was observed that the type of reinforcing bars, the length of the steel fibers, and the depth of the steel fiber-reinforced concrete layer had almost no effect on the beams' deformation behavior during the pre-cracking stage. However, depending on the aforementioned three parameters, all tested specimens showed a significant decrease in flexural stiffness, causing the deflection to increase dramatically with increasing load in the post-cracking stage.

GF2.5H/3

7.88

4.2

-17.6

12.60

7.5

-46.8

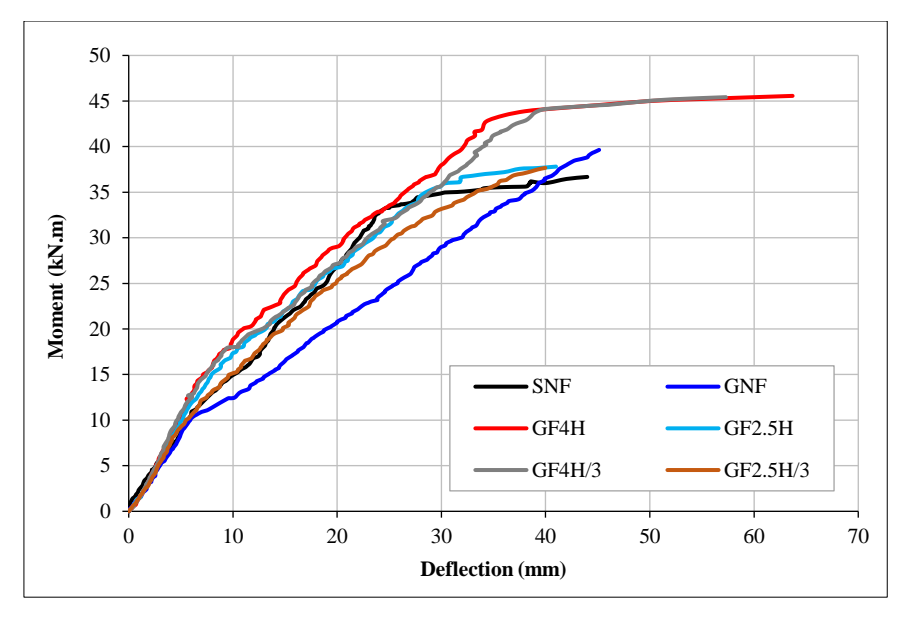


Figure 11. Moment-deflection relationship for the tested specimens

Both of the SNF and GNF tested beams showed a decrease in flexural stiffness following the cracking of the beams and up until the compression concrete was crushed. However, because GRFP is known to have a lower elastic modulus, which leads to an increase in deflections, the degradation in the flexural stiffness was more pronuncened in GNF beam.

The serviceability performance of GFRP-reinforced concrete beams was enhanced by the incorporation of discrete steel fibers; as shown in Figure 11 and Table 12, GFRP-reinforced concrete beams with steel fibers exhibited a slower reduction in bending stiffness and smaller deflections than GNF beams under the same load. Figure 11 illustrates how the application of hooked-end steel fibers of 25 mm- or 40 mm-long affects the GFRP reinforced concrete beams' deflection capacity. The improved performance of the tested GFRP-reinforced SF-reinforced concrete beams under service load was not limited to the GNF beam only. Under service moments, even when compared to the performance of SNF beam, the deformability performance of GF4H, GF2.5H, GF4H/3, and GF2.5H/3 beams almost was not exceeded the corresponding deflection values recorded for SNF beam due to the enhancement pronounced in their post-cracking flexural stiffness associated with the utilization of SF. The fibers' ability to withstand tensile strain at cracking surfaces, even at greater deflections, is attributed to their slip-hardening tendency and continually produced untwisting torque [69, 70]. Even after the flexural cracks opened widely, the beam's moment-carrying capacity did not drastically drop because of the combined impacts of the longitudinal GFRP rebars' dowel action and the 40 mm-long steel fibers' slip-hardening pullout behavior.

Corresponding cracking Beam moment			acking		responding service moment at which ximum crack width equals 0.41 mm				Corresponding service moment at which maximum crack width equals 0.50 mm				Corresponding ultimate moment		
ID	<i>M_{cr}</i> (kN.m)	Δ _{cr} (mm)	Diff. (%)	M _{ser} (kN.m)	Δ _{ser} (mm)	Diff. (%)	$\frac{L}{\Delta_{ser}}$	<i>M</i> _{ser} (kN.m)	Δ _{ser} (mm)	Diff. (%)	$\frac{L}{\Delta_{ser}}$	<i>M_u</i> (kN.m)	Δ_u (mm)	Diff. (%)	
SNF	9.00	5.1	Ref.	20.25	14.1	Ref.	85	22.50	16.5	Ref.	73	36.68	44.0	Ref.	
GNF	6.75	4.2	-17.6	10.58	6.5	-53.9	185	11.25	7.8	-52.7	154	36.95	40.8	-7.3	
GF4H	9.00	4.2	-17.6	17.33	8.8	-37.6	136	18.00	9.7	-41.2	124	45.56	٦٣,٧	+44.8	
GF2.5H	8.10	4.1	-19.6	13.73	7.3	-48.2	164	14.18	7.6	-53.9	158	37.80	41.0	-6.8	
GF4H/3	8.78	4.2	-17.6	16.65	8.6	-39.0	140	16.88	8.7	-47.3	138	45.43	57.3	+30.2	

On the other hand, the comparison of the steel fiber influence on the load-deflection relationship of tested specimens in Figure 11 demonstrated a clear improvement in behavior, bringing the moment-deflection diagrams of the GF4H, GF2.5H, GF4H/3, and GF2.5H/3 beams in the post-cracking stage closer to the behavior of the steel-reinforced concrete SNF beam.

160

13.50

8.2

-50.3

146

37.67

399

-93

Furthermore, Table 12 demonstrates the superior effect of the 40 mm long steel fiber over the 25 mm long steel fiber. When the GF4H and GF4H/3 beams were compared to the SNF beam, their peak deflections rose by 44.8% and 30.2%, respectively. The incorporation of 40 mm-long hooked-end steel fibers increased the GFRP reinforced concrete beams' ultimate deflection and deflection capacity in addition to their flexural strength.

The results shown in Figure 11 demonstrate that, for both types of steel fibers utilized, the tested GFRP-reinforced concrete beams showed a slight improvement in their deformation behaviors as the depth of the steel fiber-reinforced concrete layer increased. Under the same load, it was shown that the increased stiffness of beams GF4H and GF2.5H, which have steel fibers distributed over their entire cross-sectional depth, exhibited lesser deflections than beams GF4H/3 and GF2.5H/3, respectively.

The maximum crack widths of 0.41 mm and 0.5 mm are represented by the span-to-service load deflection ratios in Table 12. GFRP-reinforced concrete GNF beam achieves a span-to-service load deflection ratio of 185 and 154, respectively, whereas steel-reinforced concrete SNF beam achieves a ratio of 85 and 73. The corresponding ratios for GFRP-reinforced concrete beams with steel fibers, GF4H, GF2.5H, GF4H/3, and GF2.5H/3, range from (136 to 164) to (124-158). Compared to the widely recognized ratio of around (span/240), these values are comparatively high, confirming that the serviceability limit state often dictates the design of beams reinforced with GFRP bars [52].

3.6. Initial Stiffness, Energy Absorption, and Ductility Metrics

One of the key mechanical characteristics that distinguishes structural concrete members is their stiffness. It describes the structural member's resistance to deformation. Calculating stiffness mathematically involves dividing the applied force by the corresponding generated deformation. In this investigation, the initial stiffness (K) of the considered specimens was calculated by dividing the cracking load (P_{cr}) by the corresponding vertical deflection (Δ_{cr}) .

$$K = \frac{P_{cr}}{\Delta_{cr}} \tag{1}$$

Table 13 clearly shows that when GFRP bars were used for flexural reinforcement instead of steel bars, the initial stiffness dropped by 9%. Upon utilizing steel fibers, the initial stiffness of specimens GF4H and GF4H/3 was improved more than that of specimens GF2.5H and GF2.5H/3, respectively, indicating the impact of steel fiber length. Similarly, specimens GF4H and GF2.5H showed an improvement greater than that of specimens GF4H/3 and GF2.5H/3, respectively, indicating the impact of the depth of the steel fiber-containing concrete layer. The improvement in initial stiffness (K) achieved as a result of SF implementation up to 21.8% when compared to SNF and varied from 9.9% to 33.8% when compared to GNF. The pre-cracking stiffness of fibrous GFRP-reinforced concrete beams was much greater than that of steel-reinforced and non-fibrous GFRP-reinforced concrete beams, as shown in Table 13. This is explained by steel fibers' capacity to withstand tensile stress before cracking, which effectively influences the beams' neutral axis location and increases sectional stiffness. Following test specimen cracking, steel fibers that bridge across the cracks perform a "bridging" action by absorbing stresses in the form of pull-out, deformation, and fracture. This increases the beams' post-cracking stiffness, inhibits and terminates crack initiation and development, and influences the final crack distribution and pattern [71, 72].

Table 13. Absorbed energy at various loading levels for tested beams Variation (%)

Absorbed energy (kN.mm) Variation (%) @ Service load Variation (%) Variation % Beam Stiffness @ (a) Max. crack Max. crack Ref. Ref. ID (kN/m) Max. crack Crack-Max. crack Ultimate width (0.5 mm) width (0.41 mm) Ref. Ref. Ref. Ref. GNF SNF ing load width 0.5 width 0.41 load SNF **GNF** SNF **GNF** Ref. mm mm GNE SNF GNF SNF 7.8 111.9 918.9 682.7 4960.0 **GNF** 7.1 -9.0 66.4 -40.7307.0 178.5 -73.9 3783.7 -23.7 -66.6GF4H 9.0 +15.4+26.886.4 -22.8 30.1 422.6 365.7 -54.0 37.7 104.9 9613.0 93.8 154.0 -46.4 GF2.5H 8.5 +9.0 +19.770.9 -36.6 6.8 243.7 229.7 -73.5 -20.6 -66.4 28.7 4609.9 -7.1 21.8 GF4H/3 9.5 +21.8+33.875.4 -32.6 13.6 356.0 334.8 -61.3 16.0 -51.0 87.6 8092.1 113.9 63.1 GF2.5H/3 7.8 0.0 +9.9 67.1 -40.0 1.1 289.9 224.9 -68.5 -5.6 -67.1 26.0 4164.6 -16.0 10.1

The amount of energy that a material or structural member can absorb under applied load is known as its energy absorption capacity. This energy can be dissipated by fracture, plastic deformation, elastic deformation, and other processes such internal friction or damping. As shown by the test results in Table 13, the steel bars' energy absorption was much more than that of the GFRP bars. In contrast to beam SNF, the absorbed energy of beam GNF dropped by 40.7%, 73.9%, 66.6%, and 23.7% during cracking load, service load corresponding maximum crack width of 0.41 mm, service load corresponding maximum crack width of 0.5 mm, and ultimate load, respectively. The tested beam's capacity to absorb more energy and undergo plastic deformation prior to failure, (i.e., toughness), is increased when steel fibers are incorporated into the concrete matrix. In comparison to beam SNF, the absorbed energy of fibrous GFRP-reinforced concrete beams decreased during cracking load, service load corresponding maximum crack width of 0.41 mm, and service load corresponding maximum crack width of 0.5 mm, in the range of (22.8-40%), (46.4-67.1%), and (54-73.5%), respectively. Only 7.1% and 16%, respectively, of the absorbed energy was lost in GF2.5H and GF2.5H/3 under ultimate load. Under ultimate load, however, the absorbed energy in GF4H and GF4H/3 was 93.8% and 63.1% more than that of beam SNF, respectively. This is explained by the greater deflections that these beams, GF4H and GF4H/3, encountered at ultimate load (see Figure 9).

The maximum improvement in energy absorption under cracking load, service load corresponding maximum crack width of 0.41 mm, service load corresponding maximum crack width of 0.5 mm, and ultimate load was 30.1%, 104.9%, 37.7%, and 154%, respectively, according to a comparison of fibrous GFRP-reinforced concrete beams to non-fibrous GFRP beams at various loading stages.

The ability of a structural concrete beam to withstand inelastic deformation without losing its load-bearing capacity before failing is known as its ductility. Due to the brittle nature of both concrete and GFRP bars, longitudinally reinforced concrete flexural members with GFRP bars typically have a lack of ductility. This is one of the drawbacks of GFRP-reinforced concrete members. For this reason, even minor ductility improvement due to GFRP reinforcement is quite meaningful.

An indicator of ductile behavior is the ductility index. The displacement ductility index (μ_{Δ}) is commonly used to determine the ductility index of steel-reinforced concrete beams when steel exhibits obvious plastic deformation at yield (see Equation 2). It may be computed as the ratio of ultimate deflection (Δ_u) to deflection at yield (Δ_y) in steel-reinforced concrete beams.

$$\mu_{\Delta} = \frac{\Delta_u}{\Delta_y} \tag{2}$$

Although the American Guide for the Design and Construction of Structural Concrete Reinforced with Fiber-Reinforced Polymer (FRP) Bars ACI 440.1R-15 [10] and the American Building Code Requirements for Structural Concrete Reinforced with Glass Fiber-Reinforced Polymer (GFRP) Bars ACI CODE 440.11-22 [12], and the Canadian Standards for Design and Construction of Building Structures with Fibre-Reinforced Polymers (FRP) CSA-S806-12 [11] do not specify a numerical ductility index for GFRP-reinforced concrete beams, their focus is designing such structural members for adequate deformability and energy absorption capacity. By adopting over-reinforced sections and considering methods such as confining the compressive area of concrete or combining GFRP reinforcement with traditional steel reinforcement (i.e., hybrid reinforcement), designers can enhance the ductility and achieve a more favorable structural overall performance of GFRP-reinforced concrete structures. On the other hand, the Canadian Highway Bridge Design Code CSA-S6:19 [68] stipulates that concrete beams reinforced with GFRP bars or grids are required to meet a minimum displacement ductility index (μ_D) of at least 4 and 6 for rectangular and T-sections, respectively, to ensure adequate deformability before failure, considering the typical brittle nature of GFRP materials. These indices are designed to help ensure that the structure behaves in a sufficiently ductile manner under loading, which is essential for maintaining the safety and serviceability of the bridge.

Since GFRP-reinforced concrete beams lack a yield point, as up until failure their bars' stress-strain relationship is linear, the straightforward formulation of Equation 2 is inapplicable. According to the concept of ductility given above, ductility of GFRP-reinforced concrete beams may be described using either the energy-based approach or the deformation-based approach.

Mufti et al. [73], Jaeger et al. [74], Wang and Belarbi [75], and Wei et al. [76] have reported that, for concrete beams with a rectangular cross-sectional configuration and based on a particular failure mode, specifically crushing of the concrete in compression zone, the concrete strain at the extreme compression fiber is around 1000 microstrain under ultimate service load. This specific strain of 1000 microstrain is thought to mark the beginning of the inelastic deformation of concrete. Accordingly, based on the deformation-based approach, a deformation-based ductility index (μ_D) was proposed for FRP-reinforced concrete beams by Mufti et al. [73] and Jaeger et al. [74], which defines the service state using this value of compressive strain, see Equation 3. The deformation-based ductility index (μ_D) considers the full effects of strength and deflection on the ductility value.

$$\mu_D = \frac{M_u}{M_{0.001}} \frac{\Delta_u}{\Delta_{0.001}} \tag{3}$$

where M_u represents the ultimate state's moment capacity; Δ_u represents the ultimate state's deflection; $M_{0.001}$ and $\Delta_{0.001}$ represents the moment and deflection, respectively, associated with concrete strain at extreme compression fiber of 1000 microstrain.

Ductility is defined using the energy-based approach as the ratio of total energy, which comprises elastic and plastic energies $E_{tot} = (E_{el} + E_{pl})$, to elastic energy E_{el} . In their proposal, Naaman & Jeong [77] suggested using the energy balance concept to quantify the energy-based ductility index (μ_{EN}) of FRP-reinforced concrete beams, see Equation 4.

$$\mu_{EN} = \frac{1}{2} \left(\frac{E_{tot}}{E_{el}} + 1 \right) \tag{4}$$

The moment-deflection diagrams derived from testing on real beams may be used to determine the elastic energy Eel and the plastic energy E_{vl} [76, 78].

Figure 12 shows the elastic slope, S, which was developed by Naaman & Jeong [77] to quantify the elastic energy. In addition to the slopes S_1 , S_2 , and possibly S_3 , the points P_1 , P_2 , and possibly P_u must be selected in order to define an elastic slope. However, the experimental moment–deflection curves in Figure 9 do not clearly show these points. Using either Equations 5 and 6, the elastic slope S can be determined as follows:

$$S = \frac{(P_1 S_1 + (P_2 - P_1)S_2)}{P_2}$$
 for two line model (5)

$$S = \frac{(P_1 S_1 + (P_2 - P_1) S_2 + (P_u - P_2) S_3)}{P_u}$$
 for three line model (6)

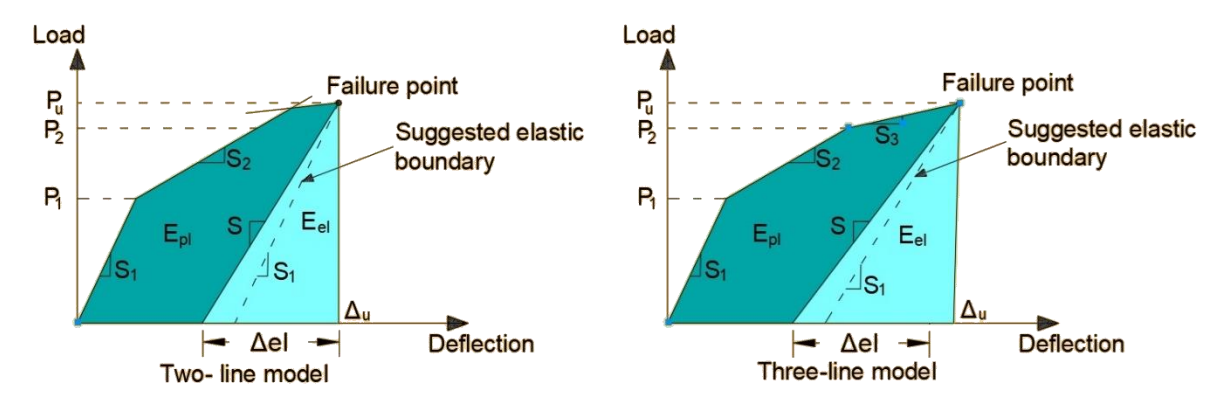


Figure 12. Schematic representation of the ductile response of a GFRP-reinforced concrete beam according to the energybased approach

In contrast to steel-reinforced concrete beams, where residual strains from plastic deformation lower the unloading slope, GFRP does not show residual strains under typical loading scenarios. Also, the matrix, which consists of steel fibers and concrete, may have slight residual deformations, but these are frequently insignificant enough to have a significant impact on the unloading stiffness. Instead of relying solely on the theoretical interpretation of earlier research studies [49,75-78], it was proposed in this study that the unloading slopes be used to depict the elastic slopes, see the dashed lines in Figure 10. The unloading curve's slope, which represents 100% of the load capacity, was thought to be parallel to the elastic slope S_1 .

Based on the test results displayed in Figure 11, a two-line model will almost accurately approximate the moment-deflection diagram of the tested beams using two linear segments, which capture the initial stiffness and post-cracking behavior until failure (i.e., characterized by beam failure and cracking). On the other hand, a three-line model will almost depict the moment-deflection diagram of the tested beams using three linear segments, which is mainly composed of the cracking point, concrete damage point, and ultimate load point.

Up to the failure load, the area under the load-deflection curve is used to compute the total energy (E_{tot}) . This area can be calculated numerically using the Trapezoidal Rule. In contrast, the area of the triangle created at failure load by unloading the beam can be used to calculate the elastic energy $(E_{el}l)$.

$$E_{el} = \frac{1}{2} P_u \Delta_{el} \tag{7}$$

$$E_{tot} \approx \sum_{i=0}^{n-1} \frac{1}{2} (\Delta_{i+1} - \Delta_i) (P_i + P_{i+1})$$
 (8)

where Δ_i and Δ_{i+1} are deflections at points i and i+1, respectively; P_i and P_{i+1} are corresponding loads, and n is the total number of data points.

An overview of the computed ductility indices is given in Table 14. It should be mentioned that the ductility index for the steel-reinforced SNF beam was determined according to Equation 2. According to Equations 5 and 6 the energy-based ductility indices of GFRP-reinforced concrete beams with steel fibers, which were computed taking into account the elastic slope, *S*, were 1.81, 1.39, 1.54, and 1.21 for beams GF4H, GF2.5H, GF4H/3, and GF2.5H/3, respectively. The energy-based ductility index for the aforementioned fibrous GFRP-reinforced beams, however, reached 2.69, 2.02, 2.58, and 1.72, correspondingly, as a result of using the suggested unloading slopes to represent the elastic slopes, which decreased the elastic energy. The advantages of adding fibers to concrete, such as the increase in ultimate moment capacity and the corresponding increase in deflection, cannot be effectively considered by the energy-based approach [75]. Unlike the energy-based approach, the deformation-based ductility index proposed by Jaeger et al. [74] can independently reflect parameters like the load capacity and the impact of deformation on ductility. In the meanwhile,

the calculations showed that μ_D achieved for GF4H, GF2.5H, GF4H/3, and GF2.5H/3, respectively, 6.9, 4.8, 6.3, and 4.2, i.e., every ductility index determined for fibrous GFRP-reinforced concrete beams using Jaeger's approach was higher than the required minimum of 4 [68, 74]. There are significant differences in the ductility indices calculated using the two approaches. With the energy-based approach that considered the elastic slope of Equations 5 and 6, the energy-based approach that considered the proposed unloading slopes for representing the elastic slopes, and the deformation-based approach, the average value for the ductility index for the fibrous GFRP-reinforced concrete beams was 1.49, 2.25, and 5.55, respectively. Worthy to note that, comparing the different average results of the ductility indices for the fibrous GFRP-reinforced concrete beams to that of the non-fibrous GFRP-reinforced beam GNF showed the remarkable impact of the steel fiber, where the enhancement attained 27.1%, 52.2%, and 122%, respectively, using the aforementioned approaches. This finding indicates that the deformation-based approach has a significantly stronger impact on the ductility indices due to the incorporation of steel fibers in the concrete matrix.

From Table 14, it is evident that, in comparison to the total cross-sectional depth of the beam, the length of the steel fibers has a greater influence on the enhancement of ductility than does the depth of the layer at which the fibers are distributed.

Beam .	Energy-based ductility index according to Naaman & Jeong [77]						an & Jeo		index accorroposed ac energy		Deformation-based ductility index according to Jaeger et al. [74]								
ID								Variat	ion (%)				Variat	tion (%)	м	Λ		Variat	ion (%)
	E_{tot}	E_{el}	μ_{EN}	Ref. (SNF)	Ref. (GNF)	E_{tot}	E_{el}	μ_{EN}	Ref. (SNF)	Ref. (GNF)	M _{0.001} (kN.m)	$\frac{\Delta_{0.001}}{(\mathbf{mm})}$	μ_D	Ref. (SNF)	Ref. (SNF)				
SNF			3.5	Ref.				3.5	Ref.				3.5	Ref.					
GNF	3784	2832.4	1.17	-66.6	Ref.	3784	1929	1.48	-57.7	Ref.	24.5	25	2.5	-29.5	Ref.				
GF4H	9613	3662.0	1.81	-48.2	55.2	9613	2197	2.69	-23.1	81.8	25.6	16.4	6.9	98.0	180.8				
GF2.5H	4610	2602.7	1.39	-60.4	18.6	4610	1512	2.02	-42.3	36.5	21.9	14.8	4.8	36.9	94.3				
GF4H/3	8092	3909.2	1.54	-56.1	31.4	8092	1948	2.58	-26.3	74.3	24.3	17.0	6.3	80.5	156.0				
GF2.5H/3	4165	2935.3	1.21	-65.4	3.6	4165	1833	1.72	-50.9	16.2	21.9	16.4	4.2	19.8	70.0				

Table 14. Ductility index for tested beams

3.7. Strain Development in Concrete and GFRP Bars Under Applied Load

The strain profile for each tested beam's midspan section under a service loading stage that delivered a bending moment of 8.5 kN.m is shown in Figure 13, where the plane section assumption is satisfied by the assumed linear strain distribution. A closer look to the strain variations in the concrete's compression and tension zones revealed that the strain difference in both zones of the SNF and GNF tested beams is comparatively significant. The concrete in the tension zone was where this difference was most noticeable, resulting from the GFRP bars' reduced modulus of elasticity. Nevertheless, adding steel fibers results in a noticeable improvement in the distribution behavior of normal strain by improving the uniformity of concrete strain under compression and tension effects. The ability of steel fibers to bridge cracks and disperse stresses more uniformly throughout the concrete matrix is the reason behind this fact.

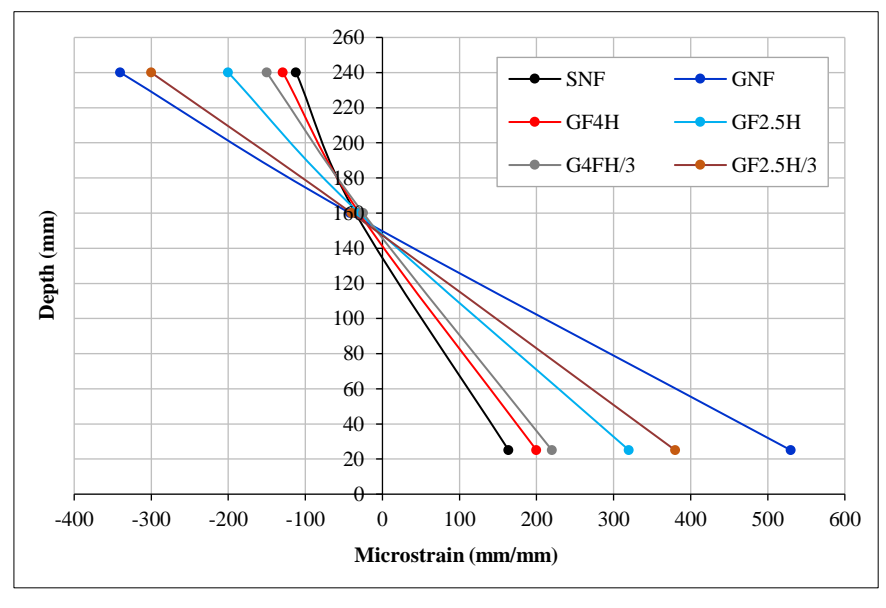


Figure 13. Midspan section strain profile across the depth of the tested specimens at a bending moment of 8.5 kN.m

Comparatively, the influence of modifying concrete tensile uniformity and increasing load bearing capacity is better with longer steel fibers. As shown in Figure 13, the close behavior of specimens SNF, GF4H, and GF4H/3 was clearly visible. Investigating Figure 11 reveals that, at a service bending moment of 8.5 kN.m, the SNF beam exhibited the smallest compression zone depth (130 mm), while the GNF beam had the largest (150 mm). The remaining specimens fell in between, following this order: GF4H (140 mm), GF4H/3 (145 mm), GF2.5H (148 mm), and GF2.5H/3 (149 mm). Figure 14 illustrates the correlations between the applied bending moment and the longitudinal bar normal strains for each tested beam. Before cracking, all of the diagrams often display comparable moment-strain correlations. Then, as the load increased, a more noticeable strain progress was observed, which was accompanied by the post-cracking stiffness decreasing. Subsequently, notable variations were noted depending on the kind of reinforcements employed. In contrast to the SNF, GF4H, GF2.5H, and GF4H/3 beams, which displayed a trilinear moment-strain relationship, the GNF and GF2.5H/3 beams exhibited a typical bilinear interaction.

Under the same service load, which corresponded to a maximum crack width of 0.41 mm or 0.5 mm, the longitudinal bars' tensile strains increased in the following order: SNF, GF4H, GF4H/3, GF2.5H, GF2.5H/3, and GNF, see Table 15. This observation underscores the dominant effect of steel fiber length in influencing performance, alongside the depth at which the fibers are distributed within the beam's cross-section (Figure 14).

Beam ID	Normal strain and its variations corresponding to											
	Cracking moment (με)	Variation (%)		Service moment		Variation%						
				Max. crack	Max.	Max. crack width of 0.41 mm		Max. crack width of 0.5 mm		Ultimate moment	Variation (%)	
		Ref. (SNF)	Ref. (GNF)	- width of 0.41 mm (με)	Crack width of $0.5 \text{ mm } (\mu \varepsilon)$	Ref. (SNF)	Ref. (GNF)	Ref. (SNF)	Ref. (GNF)	(με)	Ref. (SNF)	Ref. (GNF)
SNF	408			2800	3100					14858		
GNF	730	+78.9		6183	6520	+120.8		+110.3		18041	+21.4	
GF4H	280	-31.4	-61.6	3061	3276	+9.3	-50.5	+5.7	-49.8	20100	+35.3	+11.4
GF2.5H	560	+37.3	-23.3	3805	4055	+35.9	-38.5	+30.8	-37.8	17000	+14.4	-5.8
GF4H/3	435	+6.6	-40.4	3634	3750	+29.8	-41.2	+21.0	-42.5	18579	+25.0	+3.0
GF2.5H/3	631	+54.7	-13.6	3961	4561	+41.5	-35.9	+47.1	-30.0	17661	+18.9	-2.1

Table 15. Normal strain of flexural reinforcement at different loading stages

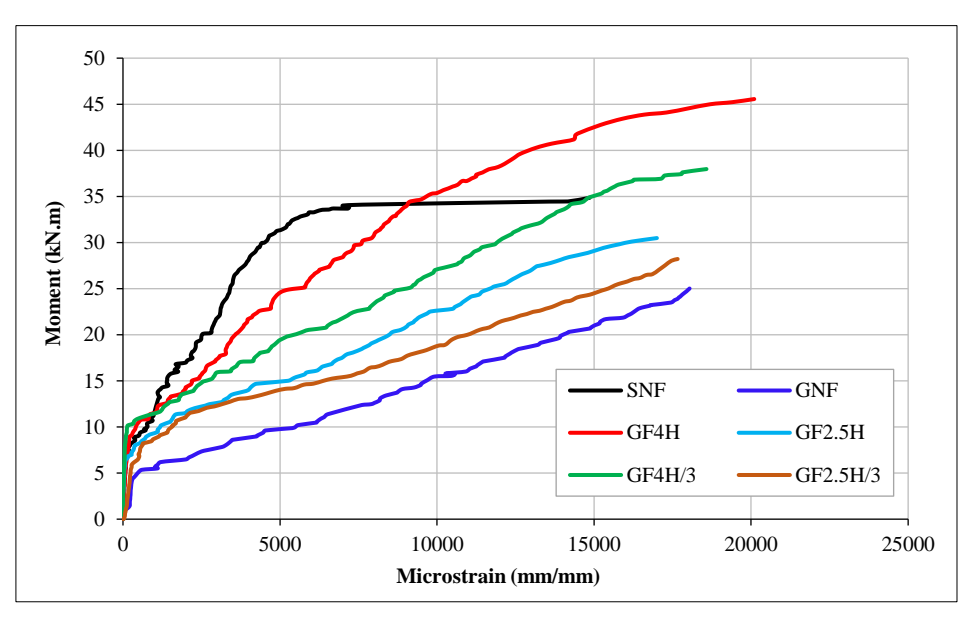


Figure 14. Strain development in tensile GFRP bars during loading

This can be attributed to the increased cracking moment caused by the steel fibers being incorporated into the concrete matrix. Despite a similar increase in the slope of the moment-strain curves for GFRP-reinforced concrete beams with steel fibers, the GF2.5H and GF2.5H/3 beams experienced higher rebar strains at the same post-cracking moment due to their wider flexural cracks compared to the GF4H and GF4H/3 beams. This is due to the fact that pulling out the 40 mm-long steel fibers from the surrounding concrete required a greater applied load at the crack planes than it did for the 25 mm-long fibers. As evidenced by the normal strain results at the ultimate stage, the use of 40 mm-long fibers effectively limited strain development in the flexural reinforcement and restricted crack widening, leading to increased maximum bending moment and deflection capacity in the reinforced concrete beams.

The GNF beam's GFRP bars experienced greater strain than the SNF beam's steel bars at the cracking moment and service moment, which corresponded to maximum crack widths of 0.41 mm and 0.5 mm, respectively. As shown in Table 15, the variance was 78.9%, 120.8%, and 110.3%. Compared to the cracking stage, the strain difference between the GFRP bars in the GNF beam and the steel bars in the SNF specimen was larger at the service stage. This is because GFRP bars undergo an enormous strain increase than steel bars to balance the applied load due to their higher flexibility (i.e., lower stiffness) after cracking. When steel fibers were introduced, this variance decreased; however, the amount of variation differed from specimen to specimen. The GF4H specimen demonstrated the optimal case, with the strain variation corresponding to the SNF beam being -31.4%, +9.3%, and +5.7% during the cracking and service loading phases, respectively.

4. Conclusions

This study investigated experimentally the impact of steel fiber length and a steel fiber-reinforced concrete layer on the structural performance of GFRP-reinforced beams related to steel-reinforced beams. The key findings are as follows:

- In contrast to previous studies, the addition of 1.25% steel fibers significantly enhanced the ultimate moment capacity, with GFRP-reinforced beams achieving up to 24.2% higher strength than their steel-reinforced counterparts. The added cost of steel fibers—approximately 3–4 USD per kilogram—is minimal compared to the substantial improvement in the structural performance of the GFRP-reinforced beams.
- The cracking moment of GFRP-reinforced beams was initially 25% lower than that of steel-reinforced beams due to varied bonding behavior, lower modulus of elasticity, anisotropy, and reduced stiffness of the GFRP bars. However, adding 40 mm-long steel fibers significantly improved cracking resistance, reaching just 2.5% below steel-reinforced beams and increasing by 16.67%—33.33% compared to non-fibrous GFRP beams.
- The bridging ability of the hooked-end steel fibers enhanced the shear resistance of GFRP-reinforced beams by improving the concrete's compressive and tensile strength, effectively controlling crack formation and preventing shear crack widening.
- The steel fiber length had a slight impact on crack spacing, but increasing the depth of the fiber-reinforced concrete layer significantly improved crack control. Full-depth fiber reinforcement was more effective than partial-depth application.
- The beams with 40 mm-long steel fibers exhibited better crack width control, performing closer to steel-reinforced beams, while 25 mm-long fibers had a lesser effect. As the bridging impact was greater than that of shorter fibers, this illustrates how effectively extending the fiber length to a certain practical value may reduce crack width
- The experimental results highlight the need for reinforcement design improvements to ensure compliance with crack width limitations and serviceability standards to preserve structural integrity and durability under various environmental conditions, as current ACI 318-19 provisions may not fully align with FRP-RC behavior.
- The fiber length and the depth of the steel fiber-reinforced concrete layer had minimal impact on pre-cracking deformation but significantly influenced post-cracking stiffness. Beams with 40 mm fibers showed superior deflection control and flexural strength.
- The non-fibrous GFRP-reinforced concrete beam achieved a span-to-service load deflection ratio of 185 and 154, respectively, conforming to maximum crack widths of 0.41 mm and 0.5 mm, whereas the steel-reinforced concrete beam achieved a ratio of 85 and 73, respectively. The corresponding ratios for GFRP-reinforced concrete beams with steel fibers range from (136 to 164) to (124-158). Concerning the widely recognized ratio of around (span/240), these values are comparatively high, confirming that the serviceability limit state often dictates the design of beams reinforced with GFRP bars.
- Adding steel fibers improved energy absorption by up to 154% at ultimate load and significantly enhanced performance under various loading conditions.
- The ductility indices varied based on calculation methods but consistently showed significant improvement with steel fibers, with enhancements of up to 122% compared to non-fibrous GFRP beams.

These findings emphasize the benefits of combining steel fibers into GFRP-reinforced concrete beams to improve strength, crack resistance, and serviceability, contributing to more durable and efficient structural designs.

5. Declarations

5.1. Author Contributions

Conceptualization, N.K.O., S.D.M., R.M.A., and H.M.S.; methodology, S.D.M. and R.M.A.; formal analysis, N.K.O. and S. D.M.; investigation, A.A.A.; resources, A.A.A. and R.M.A.; data curation, S.D.M., and H.M.S.; writing—original draft preparation, S.D.M., R.M.A., and H.M.S.; writing—review and editing, N.K.O. and S.D.M.; supervision, N.K.O. and A.A.A.; funding acquisition, N.K.O., A.A.A., S.D.M., R.M.A., and H.M.S. All authors have read and agreed to the published version of the manuscript.

5.2. Data Availability Statement

The data presented in this study are available on request from the corresponding author.

5.3. Funding

The authors received no financial support for the research, authorship, and/or publication of this article.

5.4. Acknowledgements

The authors would like to express their sincere gratitude to the staff of the Structural Laboratory in the Civil Engineering Department at the University of Baghdad, Iraq, for their valuable support in the experimental phase of this research. They also extend their thanks to the Consulting Engineering Bureau at the University of Baghdad (CEB-UB) for their assistance in conducting the material tests.

5.5. Conflicts of Interest

The authors declare no conflict of interest.

6. References

- [1] Franceschini, L., Vecchi, F., Tondolo, F., Belletti, B., & Sánchez Montero, J. (2022). Mechanical behaviour of corroded strands under chloride attack: A new constitutive law. Construction and Building Materials, 316. doi:10.1016/j.conbuildmat.2021.125872.
- [2] Yardim, Y., Yilmaz, S., Corradi, M., & Thanoon, W. A. (2023). Strengthening of Reinforced Concrete Non-Circular Columns with FRP. Materials, 16(21), 6973. doi:10.3390/ma16216973.
- [3] Makhlouf, M. H., Ismail, G., Abdel Kreem, A. H., & Badawi, M. I. (2023). Investigation of transverse reinforcement for R.C flat slabs against punching shear and comparison with innovative strengthening technique using FRP ropes. Case Studies in Construction Materials, 18, 1935. doi:10.1016/j.cscm.2023.e01935.
- [4] Mohammad, A. Q., & Abbas, R. M. (2023). Structural Behavior of Prestressed RC Dapped Beam with Openings Strengthened Using CFRP Sheets. E3S Web of Conferences, 427, 1–9. doi:10.1051/e3sconf/202342702004.
- [5] El-Hassan, H., El Maaddawy, T., & Šišková, A. (2019). Microstructure Characteristics of GFRP Reinforcing Bars in Harsh Environment. Advances in Materials Science and Engineering, 2019, 8053843. doi:10.1155/2019/8053843.
- [6] Benmokrane, B., Chaallal, O., & Masmoudi, R. (1995). Glass fibre reinforced plastic (GFRP) rebars for concrete structures. Construction and Building Materials, 9(6), 353–364. doi:10.1016/0950-0618(95)00048-8.
- [7] Wu, T., Sun, Y., Liu, X., & Wei, H. (2019). Flexural behavior of steel fiber–reinforced lightweight aggregate concrete beams reinforced with glass fiber–reinforced polymer bars. Journal of Composites for Construction, 23(2), 04018081. doi:10.1061/(ASCE)CC.1943-5614.0000920.
- [8] Saikia, B., Kumar, P., Thomas, J., Rao, K. S. N., & Ramaswamy, A. (2007). Strength and serviceability performance of beams reinforced with GFRP bars in flexure. Construction and Building Materials, 21(8), 1709–1719. doi:10.1016/j.conbuildmat.2006.05.021.
- [9] Issa, M. S., Metwally, I. M., & Elzeiny, S. M. (2011). Influence of fibers on flexural behavior and ductility of concrete beams reinforced with GFRP rebars. Engineering Structures, 33(5), 1754–1763. doi:10.1016/j.engstruct.2011.02.014.
- [10] ACI 440.1R-15. (2015). Guide for the Design and Construction of Structural Concrete Reinforced with Fiber-Reinforced Polymer (FRP) Bars. American Concrete Institute (ACI), Farmington Hills, United States.
- [11] CSA S806:12 (R2021). (2021). Design and Construction of Building structures with Fibre-Reinforced Polymer. Canadian Standards Association (CSA), Toronto, Canada.
- [12] ACI CODE-440.11-22. (2022). Building Code Requirements for Structural Concrete Reinforced with Glass Fiber-Reinforced Polymer (GFRP) Bars—Code and Commentary. American Concrete Institute (ACI), Farmington Hills, United States.
- [13] Alsayed, S. H., Al-Salloum, Y. A., & Almusallam, T. H. (2000). Performance of glass fiber reinforced plastic bars as a reinforcing material for concrete structures. Composites Part B: Engineering, 31(6–7), 555–567. doi:10.1016/S1359-8368(99)00049-9.
- [14] Tavares, D. H., Giongo, J. S., & Paultre, P. (2008). Behavior of reinforced concrete beams reinforced with GFRP bars. Revista IBRACON de Estruturas e Materiais, 1(3), 285–295. doi:10.1590/s1983-41952008000300004.
- [15] Pecce, M., Manfredi, G., & Cosenza, E. (2000). Experimental Response and Code Models of GFRP RC Beams in Bending. Journal of Composites for Construction, 4(4), 182–190. doi:10.1061/(asce)1090-0268(2000)4:4(182).

- [16] Toutanji, H. A., & Saafi, M. (2000). Flexural behavior of concrete beams reinforced with glass fiber-reinforced polymer (GFRP) bars. ACI Structural Journal, 97(5), 712–719. doi:10.14359/8806.
- [17] Rasheed, H. A., Nayal, R., & Melhem, H. (2004). Response prediction of concrete beams reinforced with FRP bars. Composite Structures, 65(2), 193–204. doi:10.1016/j.compstruct.2003.10.016.
- [18] Yost, J. R., & Gross, S. P. (2002). Flexural design methodology for concrete beams reinforced with fiber-reinforced polymers. ACI Structural Journal, 99(3), 308–316. doi:10.14359/11914.
- [19] Adam, M. A., Said, M., Mahmoud, A. A., & Shanour, A. S. (2015). Analytical and experimental flexural behavior of concrete beams reinforced with glass fiber reinforced polymers bars. Construction and Building Materials, 84, 354–366. doi:10.1016/j.conbuildmat.2015.03.057.
- [20] Naveen Kumar, G., & Sundaravadivelu, K. (2017). Experimental Study On Flexural Behaviour Of Beams Reinforced With GFRP Rebars. IOP Conference Series: Earth and Environmental Science, 80, 012027. doi:10.1088/1755-1315/80/1/012027.
- [21] Saraswathy, T., & Dhanalakshmi, K. (2014). Investigation of flexural behaviour of RCC beams using GFRP bars. International Journal of Scientific & Engineering Research, 5(1), 333-338.
- [22] Moawad, M. S., & Fawzi, A. (2021). Performance of concrete beams partially/fully reinforced with glass fiber polymer bars. Journal of Engineering and Applied Science, 68(1), 1–18. doi:10.1186/s44147-021-00028-6.
- [23] Rasheed, M. R., & Mohammed, S. D. (2024). Structural Behavior of Concrete One-Way Slab with Mixed Reinforcement of Steel and Glass Fiber Polymer Bars under Fire Exposure. Engineering, Technology and Applied Science Research, 14(2), 13380–13387. doi:10.48084/etasr.6795.
- [24] Rasheed, M. R., & Mohammed, S. D. (2024). Structural behavior of one-way slabs reinforced by a combination of GFRP and steel bars: An experimental and numerical investigation. Journal of the Mechanical Behavior of Materials, 33(1), 20240002. doi:10.1515/jmbm-2024-0002.
- [25] Liang, X., Peng, J., & Ren, R. (2023). A state-of-the-art review: Shear performance of the concrete beams reinforced with FRP bars. Construction and Building Materials, 364. doi:10.1016/j.conbuildmat.2022.129996.
- [26] Swamy, R. N., & Al-Noori, K. A. (1975). Flexural behavior of fiber concrete with conventional steel reinforcement. Proceedings RILEM Symposium on Fiber Reinforced Cement and Concrete, 14-17 September, 1975, London, United Kingdom.
- [27] Ahmed, W., & Lim, C. W. (2021). Production of sustainable and structural fiber reinforced recycled aggregate concrete with improved fracture properties: A review. Journal of Cleaner Production, 279. doi:10.1016/j.jclepro.2020.123832.
- [28] Shen, W., Chen, S., & Zhang, J. (2022). Calculation of Cracks in Partially Steel Fiber Reinforced Concrete Beams with BFRP Bars. Advances in Materials Science and Engineering, 2022, 1–12,. doi:10.1155/2022/9158379.
- [29] Tiberti, G., Germano, F., Mudadu, A., & Plizzari, G. A. (2018). An overview of the flexural post-cracking behavior of steel fiber reinforced concrete. Structural Concrete, 19(3), 695–718. doi:10.1002/suco.201700068.
- [30] Ding, Y., Yu, K. Q., Yu, J. tao, & Xu, S. lang. (2018). Structural behaviors of ultra-high performance engineered cementitious composites (UHP-ECC) beams subjected to bending-experimental study. Construction and Building Materials, 177, 102–115. doi:10.1016/j.conbuildmat.2018.05.122.
- [31] He, F., Biolzi, L., Carvelli, V., & Monteiro, P. J. M. (2022). Digital imaging monitoring of fracture processes in hybrid steel fiber reinforced concrete. Composite Structures, 298, 116005. doi:10.1016/j.compstruct.2022.116005.
- [32] Yoo, D. Y., Yoon, Y. S., & Banthia, N. (2015). Predicting the post-cracking behavior of normal- and high-strength steel-fiber-reinforced concrete beams. Construction and Building Materials, 93, 477–485. doi:10.1016/j.conbuildmat.2015.06.006.
- [33] Qu, S., Zhang, Y., Zhu, Y., Huang, L., Qiu, M., & Shao, X. (2020). Prediction of tensile response of UHPC with aligned and ZnPh treated steel fibers based on a spatial stochastic process. Cement and Concrete Research, 136, 106165. doi:10.1016/j.cemconres.2020.106165.
- [34] Lee, S. K., Oh, T., Banthia, N., & Yoo, D. Y. (2023). Optimization of fiber aspect ratio for 90 MPa strain-hardening geopolymer composites (SHGC) with a tensile strain capacity over 7.5%. Cement and Concrete Composites, 139, 105055. doi:10.1016/j.cemconcomp.2023.105055.
- [35] Chun, B., Oh, T., Choi, H. J., Lee, S. K., Banthia, N., & Yoo, D. Y. (2023). Self-healing capacity of ultra-rapid-hardening fiber-reinforced cementitious composites under tension. Construction and Building Materials, 385, 131464. doi:10.1016/j.conbuildmat.2023.131464.
- [36] Schupack, M. (1985). Durability of SFRC exposed to severe environments. Proceedings, Steel Fiber Concrete US-Sweden Joint Seminar (NSF-STU), 3-5 June, 1985, Stockholm, Sweden.

- [37] Adnan Hadi, M., & Mohammed, S. D. (2021). Improving torsional Flexural resistance of concrete beams reinforced by hooked and straight steel fibers. Materials Today: Proceedings, 42, 3072–3082. doi:10.1016/j.matpr.2020.12.1046.
- [38] Ismael, T. M., & Mohammed, S. D. (2021). Structural performance of fiber-reinforced lightweight concrete slabs with expanded clay aggregate. Materials Today: Proceedings, 42, 2901–2908. doi:10.1016/j.matpr.2020.12.746.
- [39] Abbas, R. M., & Rakaa, R. K. (2023). Structural Performance of Lightweight Fiber Reinforced Polystyrene Aggregate Self-Compacted Concrete Beams. Engineering, Technology & Applied Science Research, 13(5), 11865–11870. doi:10.48084/etasr.6217.
- [40] Yoo, D. Y., Soleimani-Dashtaki, S., Oh, T., Chun, B., Choi, J. S., Banthia, N., & Yoon, Y. S. (2024). Effects of amount and geometrical properties of steel fiber on shear behavior of high-strength concrete beams without shear reinforcement. Cement and Concrete Composites, 151, 105606. doi:10.1016/j.cemconcomp.2024.105606.
- [41] Joshi, S. S., Thammishetti, N., & Prakash, S. S. (2018). Efficiency of steel and macro-synthetic structural fibers on the flexure-shear behaviour of prestressed concrete beams. Engineering Structures, 171, 47–55. doi:10.1016/j.engstruct.2018.05.067.
- [42] Meda, A., Minelli, F., & Plizzari, G. A. (2012). Flexural behaviour of RC beams in fibre reinforced concrete. Composites Part B: Engineering, 43(8), 2930–2937. doi:10.1016/j.compositesb.2012.06.003.
- [43] Yoo, D. Y., Banthia, N., & Yoon, Y. S. (2016). Flexural behavior of ultra-high-performance fiber-reinforced concrete beams reinforced with GFRP and steel rebars. Engineering Structures, 111, 246–262. doi:10.1016/j.engstruct.2015.12.003.
- [44] Ferrier, E., Michel, L., Zuber, B., & Chanvillard, G. (2015). Mechanical behaviour of ultra-high-performance short-fibre-reinforced concrete beams with internal fibre reinforced polymer bars. Composites Part B: Engineering, 68, 246–258. doi:10.1016/j.compositesb.2014.08.001.
- [45] Yang, J. M., Min, K. H., Shin, H. O., & Yoon, Y. S. (2012). Effect of steel and synthetic fibers on flexural behavior of high-strength concrete beams reinforced with FRP bars. Composites Part B: Engineering, 43(3), 1077–1086. doi:10.1016/j.compositesb.2012.01.044.
- [46] Yoo, D. Y., Banthia, N., & Yoon, Y. S. (2016). Predicting service deflection of ultra-high-performance fiber-reinforced concrete beams reinforced with GFRP bars. Composites Part B: Engineering, 99, 381–397. doi:10.1016/j.compositesb.2016.06.013.
- [47] Abdulmuttalib Issa, M., Allawi, A. A., & Oukaili, N. (2024). Performance of doubly reinforced concrete beams with GFRP bars. Journal of the Mechanical Behavior of Materials, 33(1), 1–14. doi:10.1515/jmbm-2022-0308.
- [48] Issa, M. A., Allawi, A. A., & Oukaili, N. (2024). Effects of GFRP Stirrup Spacing on the Behavior of Doubly GFRP-Reinforced Concrete Beams. Civil Engineering Journal (Iran), 10(2), 502–520. doi:10.28991/CEJ-2024-010-02-011.
- [49] Li, X., Zhang, W., Zhang, C., Liu, J., Li, L., & Wang, S. (2024). Flexural behavior of GFRP and steel bars reinforced lightweight ultra-high performance fiber-reinforced concrete beams with various reinforcement ratios. Structures, 70, 107897. doi:10.1016/j.istruc.2024.107897.
- [50] Qu, W., Zhang, X., & Huang, H. (2009). Flexural Behavior of Concrete Beams Reinforced with Hybrid (GFRP and Steel) Bars. Journal of Composites for Construction, 13(5), 350–359. doi:10.1061/(asce)cc.1943-5614.0000035.
- [51] Araba, A. M., & Ashour, A. F. (2018). Flexural performance of hybrid GFRP-Steel reinforced concrete continuous beams. Composites Part B: Engineering, 154, 321–336. doi:10.1016/j.compositesb.2018.08.077.
- [52] Al-Osta, M. A., Isa, M. N., Baluch, M. H., & Rahman, M. K. (2017). Flexural behavior of reinforced concrete beams strengthened with ultra-high performance fiber reinforced concrete. Construction and Building Materials, 134, 279-296. doi:10.1016/j.conbuildmat.2016.12.094.
- [53] Mazaheripour, H., Barros, J. A. O., Soltanzadeh, F., & Sena-Cruz, J. (2016). Deflection and cracking behavior of SFRSCC beams reinforced with hybrid prestressed GFRP and steel reinforcements. Engineering Structures, 125, 546–565. doi:10.1016/j.engstruct.2016.07.026.
- [54] ASTM C150/C150M-21. (2022). Standard Specification for Portland Cement. ASTM International, Pennsylvania, United States. doi:10.1520/C0150_C0150M-21.
- [55] ASTM C33/C33M-24a. (2024). Standard Specification for Concrete Aggregates. ASTM International, Pennsylvania, United States. doi:10.1520/C0033_C0033M-24A.
- [56] ASTM C1240-20. (2020). Standard Specification for Silica Fume Used in Cementitious Mixtures. ASTM International, Pennsylvania, United States. doi:10.1520/C1240-20.
- [57] ASTM C494/C494M-19. (2022). Standard Specification for Chemical Admixtures for Concrete. ASTM International, Pennsylvania, United States. doi:10.1520/C0494_C0494M-19.

- [58] ASTM A615/A615M-05a. (2017). Standard Specification for Deformed and Plain Carbon-Steel Bars for Concrete Reinforcement. ASTM International, Pennsylvania, United States. doi:10.1520/A0615_A0615M-05A.
- [59] EFNARC. (2005). European Guidelines for Self-Compacting Concrete, Specifications, Production and Use. EFNARC, Flums, Switzerland.
- [60] ASTM C39/C39M-21. (2023). Standard Test Method for Compressive Strength of Cylindrical Concrete Specimens. ASTM International, Pennsylvania, United States. doi:10.1520/C0039_C0039M-21.
- [61] ASTM C496/C496M-17. (2017). Standard Test Method for Splitting Tensile Strength of Cylindrical Concrete Specimens. ASTM International, Pennsylvania, United States. doi:10.1520/C0496_C0496M-17.
- [62] ASTM C469/C469M-22. (2022). Standard Test Method for Static Modulus of Elasticity and Poisson's Ratio of Concrete in Compression. ASTM International, Pennsylvania, United States. doi:10.1520/C0469_C0469M-22.
- [63] Yoo, D. Y., Yoon, Y. S., & Banthia, N. (2015). Flexural response of steel-fiber-reinforced concrete beams: Effects of strength, fiber content, and strain-rate. Cement and Concrete Composites, 64, 84–92. doi:10.1016/j.cemconcomp.2015.10.001.
- [64] Wegian, F. M., & Abdalla, H. A. (2005). Shear capacity of concrete beams reinforced with fiber reinforced polymers. Composite Structures, 71(1), 130–138. doi:10.1016/j.compstruct.2004.10.001.
- [65] Said, M., Adam, M. A., Mahmoud, A. A., & Shanour, A. S. (2016). Experimental and analytical shear evaluation of concrete beams reinforced with glass fiber reinforced polymers bars. Construction and Building Materials, 102, 574–591. doi:10.1016/j.conbuildmat.2015.10.185.
- [66] Wang, X., Wu, Q., & Chen, W. (2023). Experimental Study on the Impact Resistance of Steel Fiber Reinforced All-Lightweight Concrete Beams under Single and Hybrid Mixing Conditions. Buildings, 13(5). doi:10.3390/buildings13051251.
- [67] ACI 318-19. (2019 Building Code Requirements for Structural Concrete (ACI 318-19) and Commentary (ACI 318R-19). American Concrete Institute (ACI), Farmington Hills, United States.
- [68] CAN/CSA-S6:19. (2019). Canadian Highway Bridge Design Code. Canadian Standards Association (CSA), Toronto, Canada.
- [69] Wille, K., & Naaman, A. E. (2012). Pullout behavior of high-strength steel fibers embedded in ultra-high-performance concrete. ACI Materials Journal, 109(4), 479–488. doi:10.14359/51683923.
- [70] Yoo, D. Y., Sohn, H. K., Borges, P. H. R., Fediuk, R., & Kim, S. (2020). Enhancing the tensile performance of ultra-high-performance concrete through strategic use of novel half-hooked steel fibers. Journal of Materials Research and Technology, 9(3), 2914–2925. doi:10.1016/j.jmrt.2020.01.042.
- [71] Islam, A., Alengaram, U. J., Jumaat, M. Z., Ghazali, N. B., Yusoff, S., & Bashar, I. I. (2017). Influence of steel fibers on the mechanical properties and impact resistance of lightweight geopolymer concrete. Construction and Building Materials, 152, 964–977. doi:10.1016/j.conbuildmat.2017.06.092.
- [72] K. Kytinou, V., E. Chalioris, C., G. Karayannis, C., & Elenas, A. (2020). Effect of Steel Fibers on the Hysteretic Performance of Concrete Beams with Steel Reinforcement—Tests and Analysis. Materials, 13(13), 2923. doi:10.3390/ma13132923.
- [73] Mufti, A. A., Newhook, J. P., & Tadros, G. (1996). Deformability versus ductility in concrete beams with FRP reinforcement. Proceedings of the 2nd International Conference on Advanced Composite Materials in Bridges and Structures, 11-14 August, 1996, Montréal, Canada.
- [74] Jaeger, L. G., Mufti, A. A., & Tadros, G. (1997). The concept of the overall performance factor in rectangular-section reinforced concrete members. Proceedings of the 3rd International Symposium on Non-Metallic (FRP) Reinforcement for Concrete Structures, 14-16 October, Sapporo, Japan.
- [75] Wang, H., & Belarbi, A. (2011). Ductility characteristics of fiber-reinforced-concrete beams reinforced with FRP rebars. Construction and Building Materials, 25(5), 2391–2401. doi:10.1016/j.conbuildmat.2010.11.040.
- [76] Wei, B., He, X., Zhou, M., Wang, H., & He, J. (2024). Experimental study on flexural behaviors of FRP and steel bars hybrid reinforced concrete beams. Case Studies in Construction Materials, 20, 2759. doi:10.1016/j.cscm.2023.e02759.
- [77] Naaman, A., & Jeong, M. (1995). 45 Structural ductility of concrete beams prestressed with FRP tendons. Non-Metallic (FRP) Reinforcement for concrete structures: Proceedings of the second international RILEM, 23-25 August, 1995, Ghent, Belgium.
- [78] Wang, H., Zhou, M., Wei, B., Wu, C., Tang, Z., Zhang, S., & He, J. (2025). Study on flexural cracking characteristics of polypropylene fiber reinforced concrete beams with BFRP bars. Case Studies in Construction Materials, 22, 4372. doi:10.1016/j.cscm.2025.e04372.